



Review

Review of mass and momentum interactions during drop impact on a liquid film

Gangtao Liang^{a,b}, Issam Mudawar^{b,*}^a Key Laboratory of Ocean Energy Utilization and Energy Conservation of Ministry of Education, School of Energy and Power Engineering, Dalian University of Technology, Dalian 116024, China^b Purdue University Boiling and Two-Phase Flow Laboratory (PU-BTPFL), School of Mechanical Engineering, 585 Purdue Mall, West Lafayette, IN 47907, USA

ARTICLE INFO

Article history:

Received 13 February 2016

Received in revised form 11 May 2016

Accepted 13 May 2016

Available online 4 June 2016

Keywords:

Drop impact

Drop spreading

Drop splashing

Ejecta

Secondary droplets

ABSTRACT

Research on liquid drop impact, especially during the past two decades, has been motivated by a need for better predictive capability in many industries. This paper will review published works concerning mass and momentum interactions during drop impact on a liquid film. First, both experimental and numerical methods for capturing the evolution of the impact will be highlighted. This will be followed by a detailed description of the impact, including formations of the ejecta sheet, crown sheet, and splashing of secondary droplets during high-velocity impact. Other topics reviewed are impact on curved wetted surfaces, multi-drop impact, and the phenomena of spreading, coalescence and rebound in low-velocity impact. Each of these phenomena is discussed in terms of underlying physical mechanisms and predictive correlations and/or models. Despite significant past efforts to understand and characterize these phenomena, it is shown that much uncertainty remains, especially in regards to the interfacial features around the drop-film neck region during the earliest stages of the impact. Recent state-of-art advances in both experimental and numerical methods are shown to play a crucial enabling role in future research. The review is concluded with recommendations concerning future work that is needed to address poorly understood and/or contradictory issues.

© 2016 Elsevier Ltd. All rights reserved.

Contents

1. Introduction	578
1.1. Drop impact applications	578
1.2. Classification of impact targets	578
1.3. Definition of liquid film	579
1.4. Dimensionless parameters governing impact dynamics on liquid films	580
1.5. Objectives of study	581
2. Experimental methods	581
3. Numerical methods	582
4. Crown sheet and splashing	583
4.1. Crown formation mechanism	583
4.2. Crown evolution	585
4.2.1. Crown diameter	585
4.2.2. Crown height	585
4.2.3. Crown angle	587
4.2.4. Crown thickness	587
4.2.5. Cavity beneath the crown	587
4.3. Splashing phenomena	588
4.3.1. Splashing types	588

* Corresponding author. Tel.: +1 (765) 494 5705; fax: +1 (765) 494 0539.

E-mail address: mudawar@ecn.purdue.edu (I. Mudawar).URL: <https://engineering.purdue.edu/BTPFL> (I. Mudawar).

Nomenclature

A^*	spreading factor for wetted sphere	We	Weber number
C	coefficient	<i>Greek symbols</i>	
D	diameter; crown diameter	α	crown's base angle
d	diameter	μ	viscosity
D^*	non-dimensional diameter	μ^*	liquid–gas viscosity ratio
f	impact frequency	ν	kinematic viscosity
Fr	Froude number	ρ	density
g	gravitational acceleration	ρ^*	liquid–gas density ratio
H	crown height	σ	surface tension
h	film thickness	τ	non-dimensional time
H^*	non-dimensional crown height	ϕ	impact angle
h^*	non-dimensional film thickness	ω	curvature ratio
K	splashing threshold parameter	<i>Subscripts</i>	
L^*	spreading factor for wetted cylinder	b	base
L_a	length scale of wall roughness	c	cavity
L_{nd}	non-dimensional length scale of wall roughness	$drop$	liquid drop
N	number of secondary drops	e	ejecta sheet
n	exponent	f	liquid
Oh	Ohnesorge number	$film$	liquid film
P	pressure	g	gas
r	radius	max	maximum
R_a	wall roughness	r	rim
Re	Reynolds number	res	residual
R_{nd}	non-dimensional wall roughness parameter	1	residual (impact) region
T	temperature	2	initial (static) film region
t	time		
v	velocity		
v^*	non-dimensional velocity		

4.3.2.	Splashing mechanisms	588
4.3.3.	Jets and secondary droplets	589
5.	Ejecta sheet, low-velocity impact and multi-drop impact	592
5.1.	Ejecta sheet	592
5.2.	Low-velocity impact	594
5.3.	Multi-drop impact	595
6.	Concluding remarks	596
	Acknowledgements	597
	References	597

1. Introduction

1.1. Drop impact applications

The fall and impact of raindrops is a common occurrence in nature that attracts much curiosity by the observer. As shown in Fig. 1, similar drop impact is witnessed in many applications found in agriculture and daily life, such as pesticide spraying of crops [1], soil and stone erosion [2], sprinkling irrigation, spilled coffee stain, and ink blot on a desk. However, scientific research on drop impact is mainly driven by its applications in industrial technology and equipment because of its favorable heat and mass transfer potential. They include fuel drop impact in the chamber of internal-combustion engines with direct fuel injection [3], saline drop impingement on heat transfer tubes in falling-film evaporators in desalination and refrigeration [4], water droplet impact on steam turbine blades, spray cooling of electronic and power devices and in fire extinguishing [5], plasma spraying, and inkjet printing [6,7].

1.2. Classification of impact targets

In general, impact targets can be classified into (1) dry solid surface, (2) thin liquid film (also termed pre-wet surface) and (3) deep

liquid pool [8], and the collision dynamics of the drop can be vastly different, depending on the impact target [9–11]. Even though the splash morphology on a solid surface may seem similar to that on a liquid film, the underlying mechanisms for the two surface targets are fundamentally different [12]. For example, high viscosity acts to promote splashing on a dry surface, but is relegated to a secondary role on a thin film [13]. Formation of a liquid crown or splashing on a film requires lower impact energy [14,15], but the duration of subsequent disintegration is much longer than that on a dry surface [16]. And, while impact on a solid surface or liquid pool involves only drop–solid or drop–liquid interactions, respectively, drop impact on a thin film involves far more complex drop–liquid–solid interactions. Therefore, developing a fundamental understanding of drop impact can benefit greatly from treating impact targets separately, and paying special attention to the liquid film target. Interestingly, there is experimental evidence that a spray impacting even a dry surface would spread a wavy liquid film upon the surface [17,18]. Therefore, findings related to drop impact on a liquid film are expected to have broader implications to dry surface situations as well.

The mechanisms of drop impact have been reviewed by Rein [11], Yarin [19] and Moreira et al. [20] for all three types of impact targets. Other reviews include an article by Prosperetti and Oguz

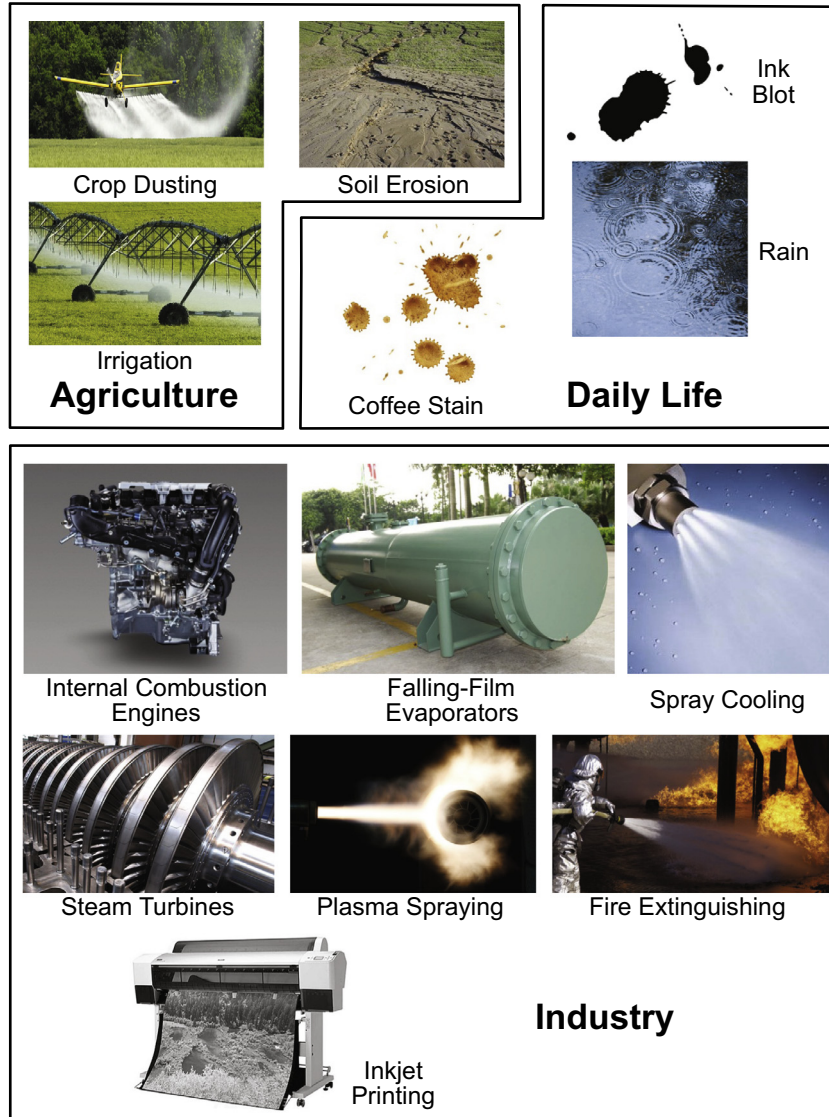


Fig. 1. Examples of drop impact in agriculture, industry and daily life.

[21] addressing pre-1993 liquid pool impact, and solid surface impact by Josserand and Thoroddsen [8]. Unlike these reviews, the present study will focus mostly on the complexities of drop impact on a thin film, and also include aspects of droplet impact on a liquid pool bearing similarities with those on a thin film. The present study will also address topics that have received little attention in prior reviews, such as multi-drop impact, to identify pressing needs for further research. Moreover, given the virtual absence of literature on heat transfer during drop impact on a thin film, this study will focus on the fluid mechanics of this type of impact.

1.3. Definition of liquid film

Before addressing the mechanism of drop impact on a thin film, it is important to determine how a thin liquid film is defined. Tropea and Marengo [22] identified four different types of liquid surfaces: thin film, liquid film, shallow pool, and deep pool. As shown in Table 1, their classification of liquid surfaces is based on the magnitude of film thickness, h , relative to arithmetical mean value

of wall roughness, R_a , and length scale of the wall roughness, L_a , where all three parameters are non-dimensionalized by the drop diameter, d_{drop} , prior to impact,

$$h^* = h/d_{drop}, \tag{1a}$$

$$R_{nd} = R_a/d_{drop}, \tag{1b}$$

$$L_{nd} = L_a/d_{drop}. \tag{1c}$$

Table 1
Regimes of drop impact on a liquid surface [22].

Regime	Range	Impact characteristics
Thin film	$L_{nd} < h^* < 3R_{nd}^{0.16}$	Impact depends on wall features
Liquid film	$3R_{nd}^{0.16} < h^* < 1.5$	Impact is weakly dependent on wall features
Shallow pool	$1.5 < h^* < 4$	Impact depends on film thickness but is independent of wall features
Deep pool	$h^* \gg 4$	Impact is independent of film thickness

Table 1 indicates that film regimes (thin film and liquid film) are restricted to $h^* < 1.5$. Vander Wal et al. [23] recommended a different classification, with thin films corresponding to $h^* \approx 0.1$, and thick films $0.1 \leq h^* \leq 10$. Wang and Chen [24] recommended very thin film classification for $h^* < 0.1$. On the other hand, Cossali et al. [25] and Motzkus et al. [26] reported that thin films are associated with $h^* < 1$. Several investigators emphasized that wall roughness underneath the film should not be neglected for thinner films [25,27,28], typically when $Re_{nd} \approx 1$ [29,30].

1.4. Dimensionless parameters governing impact dynamics on liquid films

Fig. 2 shows various stages and types of drop impact, along with definitions and nomenclature adopted in the present study. Shown are (i) the drop prior to impact, (ii) formation of the ejecta sheet, (iii) transition from ejecta to liquid crown, (iv) formation of liquid crown following impact without splashing, and (v) formation of liquid crown following impact with splashing. The ejecta is a very

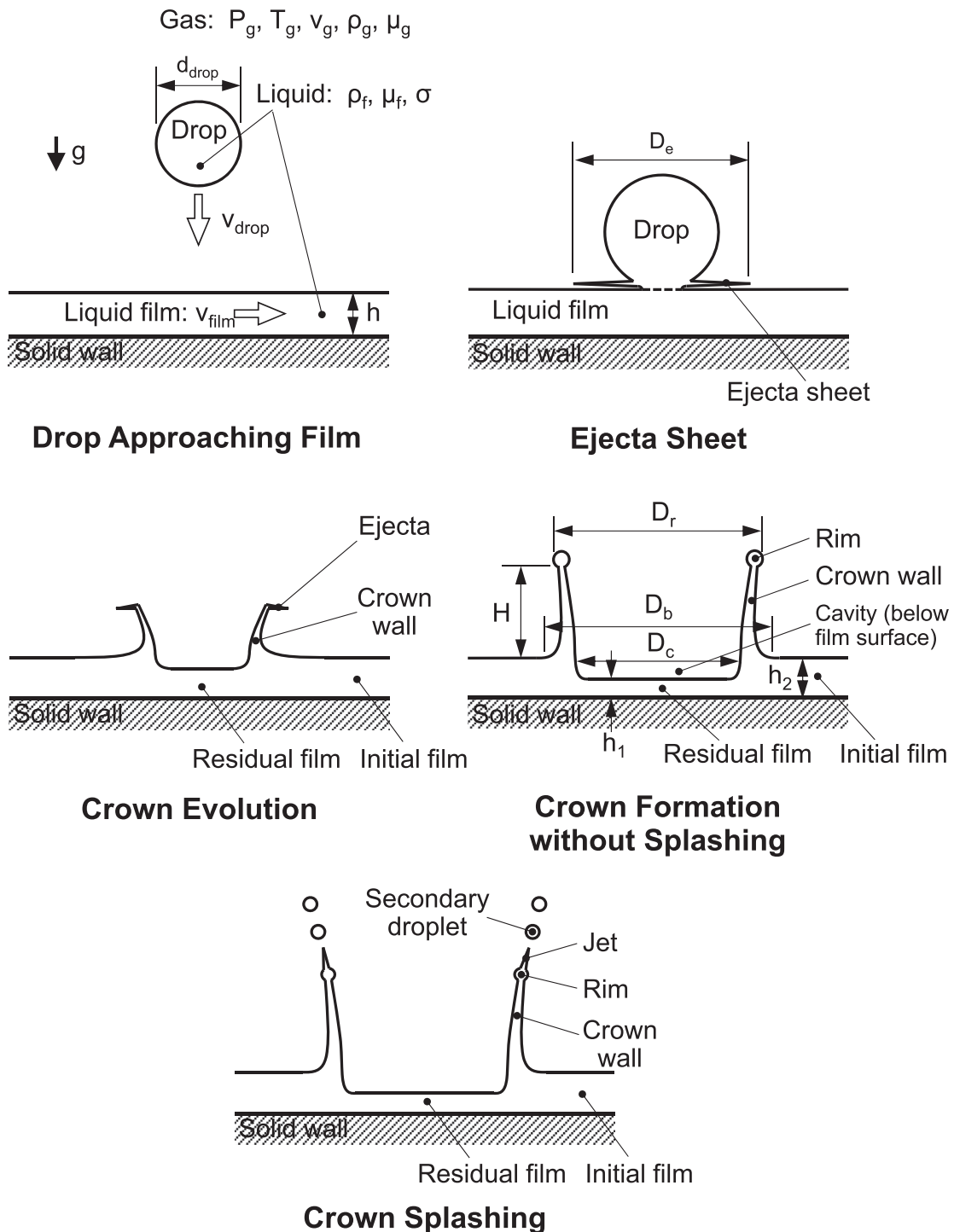


Fig. 2. Schematics of drop impact on a liquid film and associated nomenclature.

thin liquid sheet that forms in the earliest stages (first milliseconds) of impact, and which culminates in the formation of the liquid crown. Splashing refers to shattering of small secondary droplets from the crown's rim.

The main factors that influence the drop impact dynamics include the liquid drop parameters (diameter, d_{drop} , impact velocity, v_{drop} , temperature, and liquid properties of viscosity, μ_f , density, ρ_f , and surface tension, σ), the liquid film parameters (thickness, h , velocity, v_{film} , composition, temperature, and features of underlying surface), and the surrounding gas (velocity, pressure, temperature, flow regime and gas properties of viscosity, μ_g , and density, ρ_g) [19,26]. Various combinations of these parameters have been used to define non-dimensional parameters in pursuit of universal results from experiments or simulations. The most popular non-dimensional groups are:

$$We = \frac{\rho_f v_{drop}^2 d_{drop}}{\sigma}, \quad (2a)$$

$$Re = \frac{\rho_f v_{drop} d_{drop}}{\mu_f}, \quad (2b)$$

$$Oh = \frac{\mu_f}{\sqrt{\rho_f \sigma d_{drop}}}, \quad (2c)$$

$$Fr = \frac{v_{drop}^2}{g d_{drop}}, \quad (2d)$$

$$\tau = \frac{v_{drop} t}{d_{drop}}, \quad (2e)$$

where We , Re , Oh , Fr , and τ denote Weber number, Reynolds number, Ohnesorge number, Froude number, and non-dimensional time, respectively. In general, gravity effects can be neglected for $Fr \geq 10^2$ [19,31]. Two other pertinent parameters are the ratios of liquid–gas density and viscosity [32], which are defined, respectively, as

$$\rho^* = \frac{\rho_f}{\rho_g}, \quad (3a)$$

and

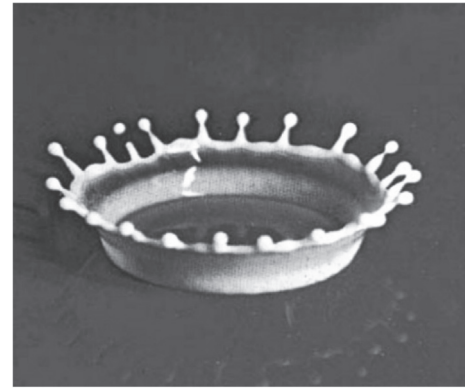
$$\mu^* = \frac{\mu_f}{\mu_g}. \quad (3b)$$

1.5. Objectives of study

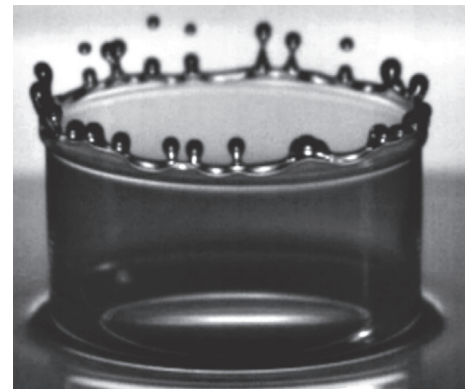
This paper will review published literature concerning mostly the fluid mechanics of a drop impacting a liquid film. Included in the review are depictions of the intermediate stages of evolution of the impact, supported by detailed identification of dominant mechanisms, and description of the experimental and/or numerical techniques used by different authors. Major topics discussed are crown sheet, ejecta sheet, and splashing for high-velocity impact. Also reviewed are impact on curved surfaces, the phenomena of spreading, coalescence and rebound associated with low-velocity impact, and multi-drop impact. The review is concluded with recommendations concerning future work that is needed to address poorly understood and/or contradictory issues.

2. Experimental methods

Since Worthington and Cole [33–35] performed their pioneering visualization experiments of drop impact over a hundred years



(a)



(b)

Fig. 3. Experimental imaging of drop splashing: (a) Edgerton's image of crown splashing of milk drop [36]. (b) Splashing captured by Deegan et al. [31] using a high-speed camera with backlighting.

ago, by employing an ordinary quarter-plate camera and very short duration electric flash to illuminate and freeze the image, the drop impact phenomenon has attracted the artistic curiosity and scientific attention of numerous researchers. In 1954, Edgerton [36] promoted very high-speed (about 10 μ s) flash photography and took the well-known photograph of milk drop crown splashing depicted in Fig. 3(a). Yet, further developments in high-speed photography had to wait until the 1960s, with most noteworthy investigations occurring during the last two decades, owing to great advances in high-speed imaging technology and ancillary equipment. In combination with high-intensity direct backlighting, high-speed cameras have enabled time-resolved imaging of drop–film interactions, including fast splashing resulting from high-velocity drop impact, as shown in Fig. 3(b). These advances are largely responsible for the recent understanding of the evolution of drop impact on a liquid film.

Thoroddsen et al. [37] reviewed the main types of high-speed cameras used in experimental fluid mechanics, including stroboscopic imaging, rotating mirror and drum cameras, beam splitter cameras, image converter cameras, and 100 billion frames per second (fps) cameras. Recently, Versluis [38] also reviewed high-speed imaging techniques in fluid mechanics, including ultra-high-speed imaging at frame rates exceeding 1 million fps. He summarized the criteria for temporal and spatial scales, which are the basis for selecting an appropriate high-speed imaging system for a given application. In general, cameras with shutter speeds up to 1 million fps are deemed sufficient to observe drop impact [39–42]. Nonetheless, the speeds cited in most publications

are no greater than 10^4 fps. Higher speeds and more sophisticated optics are required for more intricate and demanding situations, such as the capture of vortices [43], bubble entrainment [44,45] and ejecta sheet [46]. Deeney and Choi [47] used X-ray illumination to produce extremely short time scales. Zhang et al. [48] applied a phase-contrast X-ray technique to capture the ejecta, using the Advanced Photon Source at Argonne National Laboratory. Compared with the images captured by Thoroddsen [49] using an ultra-high-speed camera with dual-frame imaging and pulsed lasers, the images of Zhang et al. provide superior detail and resolution. Using the X-ray technique of Zhang et al., Lee et al. [50,51] investigated the complex details of bubble entrainment and physical origin of vortices. Phase Doppler Anemometry (PDA) [17,52,53] and the Image Analysis Technique (IAT) [54,55] have been used recently to capture the size and number of secondary droplets.

Ninomiya and Iwamoto [56] used Particle Image Velocimetry (PIV) to investigate the mechanisms of formation of Edgerton's drop milk crown. Similar measurements related to drop impact are available in [57–61]. Overall, PIV technology provides the important benefit of measuring the liquid velocity field, which is

crucial to understanding the impact process. Recently, 3D PIV technology was used in fluid mechanics measurements [62–64], and may soon become a popular tool for investigation of drop impact. An even more promising technique is high-speed holographic imaging, which is described by Thoroddsen et al. [37].

3. Numerical methods

Two-phase flows in the natural and industrial worlds involve highly complex phenomena stemming from existence and deformations of liquid–gas interfaces, which are primary reasons behind the difficulty simulating two-phase flows [65]. In fact, one of the key challenges in simulating drop impact is achieving a sharp interface.

Using the Marker and Cell (MAC) technique [66] to predict the interface, Harlow and Shannon [9] were the first to numerically simulate drop impact on a liquid film. Since then, several other numerical methods were adopted. Among those, the Volume of Fluid (VOF) method [67] has become quite popular in both 2D [68–71] and 3D simulations [72]. With this method, which conserves mass quite well, the interface lies within a control volume

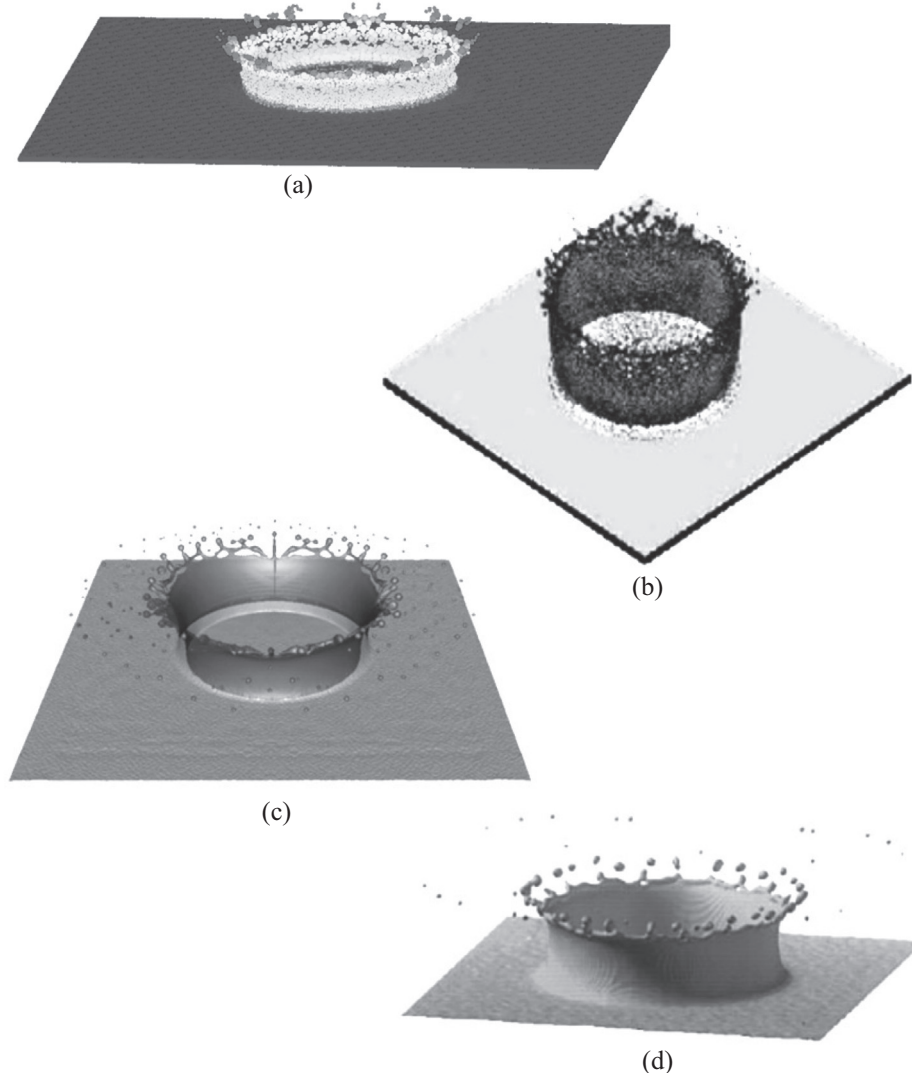


Fig. 4. 3D simulations of drop splashing on liquid films using (a) Smoothed Particle Hydrodynamics (SPH) method (Xu et al. [90]), (b) Lattice Boltzmann Method (LBM) (Shi et al. [84]), (c) Volume of Fluid (VOF) method (Nikolopoulos et al. [92]), and (d) Volume of Fluid (VOF) method (Rieber and Frohn [72]).

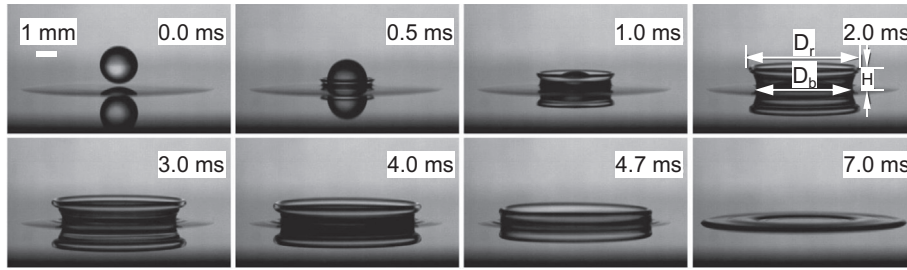


Fig. 5. Temporal record of crown liquid sheet development of butanol for $v_{drop} = 1.72$ m/s and $h^* = 0.05$ (obtained by present authors).

with a liquid volume fraction of 0–1. Its main disadvantage is that the interface normal vector and curvature are difficult to calculate, resulting in a low quality interface. Another popular method for liquid drop impact simulation is the Level Set Method (LSM) [73], applications of which are available in [74,75]. With this method, the interface is represented implicitly as a zero level set of a continuous function, providing an accurate means for calculating the interface normal vector and curvature, alas at the expense of reduced accuracy in conserving mass. Sussman and Puckett [76], and Son [77] proposed the Coupled Level Set and Volume of Fluid (CLSVOF) method to combine the advantages of the VOF and LS methods in computing incompressible two-phase flows. With the CLSVOF method, the interface normal vector and curvature are calculated using a ‘distance function’ instead of the volume fraction in the VOF method. Recent applications of the CLSVOF method in drop impact simulations can be found in [32,65,78–81].

Other methods used in drop impact simulations include the Boundary Integral Method (BIM) for scalar velocity potential [27,46], and, the Lattice Boltzmann Method (LBM) [82–86], which does not need to track or construct the gas–liquid interface. Recently, more attention has been given to Lagrangian particle methods. They include the Smoothed Particle Hydrodynamics (SPH) method [87,88] and the Moving Particle Semi-implicit (MPS) method [89]. Generally, particle methods offer two key advantages over grid-based ones. First, they can handle convection-dominated flows without numerical diffusion. Second, they are inherently well suited for simulating large deformation flows and fragmentation problems due to their mesh-free formulation, and particle method programs are relatively easy to implement. The second advantage is the key reason behind the popularity of particle methods in simulating single drop impact on a liquid film [90,91]. Fig. 4 shows 3D simulations of the splashing following drop impact on a liquid film using different numerical methods, including the Smoothed Particle Hydrodynamics (SPH) method, Fig. 4(a), Lattice Boltzmann Method (LBM), Fig. 4

(b), and Volume of Fluid (VOF) method, Fig. 4(c) and (d). The two VOF examples shown are based on different assumptions governing the influence of disturbances on the splashing process. In Fig. 4(c), disturbances are inherently induced from the drop’s motion prior to or during impingement. On the other hand, splashing in Fig. 4(d) is achieved by incorporating a random disturbance to initial velocities of the drop and film in each control volume.

4. Crown sheet and splashing

4.1. Crown formation mechanism

Fig. 5 shows evolution of the crown-like liquid sheet without splashing, which results from high energy impact. It is different

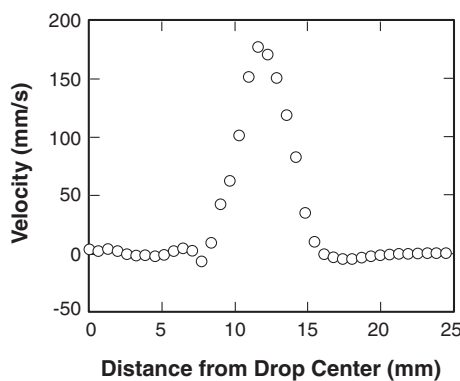


Fig. 6. PIV measurements of radial velocity during crown sheet formation in milk drop 0.0160–0.0167 s after impact for $v_{drop} = 2.43$ m/s and $h^* = 0.3125$. Adapted from Ninomiya and Iwamoto [56].

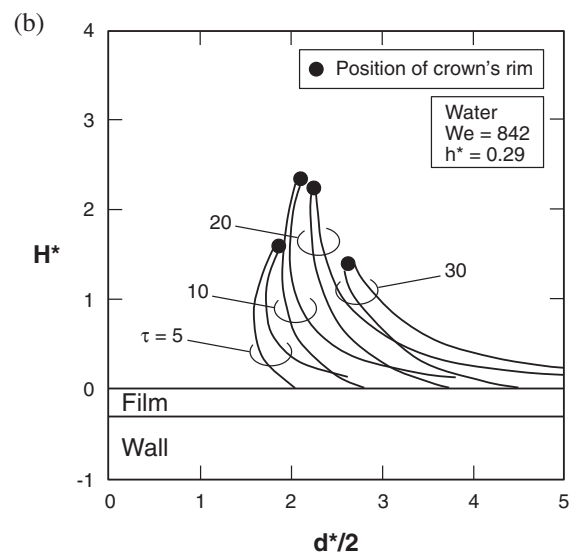
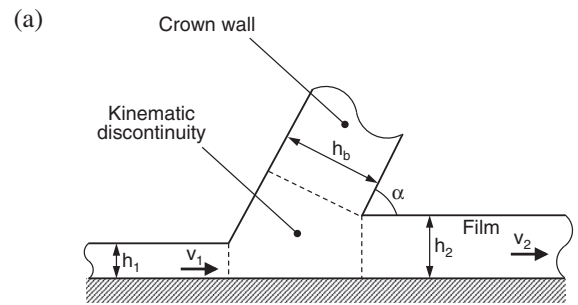


Fig. 7. (a) Schematic of crown formation based on kinematic discontinuity. (b) Predicted shape of crown evaluation for water with $We = 842$ and $h^* = 0.29$. Adapted from Roisman and Tropea [96].

from the more common crown depictions with many secondary features along the topmost rim of the crown sheet resulting from instabilities as shown earlier in Fig. 3(a) and (b). The intact shape of the crown in Fig. 5 is time dependent but not influenced by We number [72]. The crown is no longer observed for very thin films with $h^* < 0.02$ [93].

When a liquid drop collides vertically with a liquid film, the fluid inside the drop experiences a violent redirection from vertical to radial. As proposed by Yarin and Weiss [27], a kinematic discontinuity is formed as the fast redirected liquid meets the static liquid film, which contributes to the crown's formation and propagation. This theory has been widely accepted, and validated by velocity fields in both simulations [68,94] and PIV measurements [56]. Fig. 6 shows PIV measurements that clearly capture the discontinuity in liquid velocity. It should be emphasized that the theory of Yarin and Weiss does not account for viscosity effects.

Levin and Hobbs [16], Cossali et al. [25], and Liang et al. [65] all reported that crown formation is greatly influenced by film thickness, while this influence was ignored by Yarin and Weiss. Trujillo and Lee [95] adopted the concept of kinematic discontinuity but also addressed the influence of film thickness theoretically, and addressed viscous force effects by comparing predictions of the mass absorbed into the crown using viscous and inviscid assumptions. However, Roisman and Tropea [96], who ignored surface tension and viscous forces, pointed out that differences between the viscous predictions of Trujillo and Lee and inviscid predictions of Yarin and Weiss are not significant, suggesting that the main factor influencing crown formation in the case of high impact velocity is liquid inertia. Fig. 7(a) shows a Roisman and Tropea's schematic of crown formation resulting from kinematic discontinuity. In this figure, h_1 and v_1 represent film thickness and liquid velocity in the impact region, and h_2 and v_2 film thickness and liquid velocity in the static film region, respectively. The crown thickness at the base, h_b , and crown angle, α , were expressed, respectively, as

$$h_b = h_1 + h_2 \tag{4a}$$

and

$$\alpha = \arccos \left\{ \frac{(h_1 - h_2)(v_1 - v_2)^2}{h_b(v_1 - v_2)^2 - \frac{8\sigma}{\rho_f}} \right\} \tag{4b}$$

Fig. 7(b) shows analytical predictions of crown shape evolution by Roisman and Tropea for water with $We = 842$ and $h^* = 0.29$.

Several external factors have been identified that can affect crown evolution, such as surrounding gas viscosity and density [32,86,97,98], impact target geometrical shape [99,100], velocity of flowing film [39,85,101], and pre-impact shape of liquid drop [97]. Liang et al. [32] predicted an incurve of the crown with decreasing density ratio, especially for density ratios of $\mu^* < 100$, Fig. 8(a), which they attributed to large gas velocity differences between crown's upper and lower levels. They also showed that decreasing the liquid–gas viscosity ratio below $\mu^* = 0.5$ suppresses crown expansion, Fig. 8(b), because of the combined effects of pressure difference and gas velocity in the drop–film neck region. Later, Liang et al. [100] investigated drop impact on a wetted cylinder and showed that the liquid sheet almost bestrides on the cylinder surface for a curvature ratio of $\omega = 0.462$, Fig. 9, but

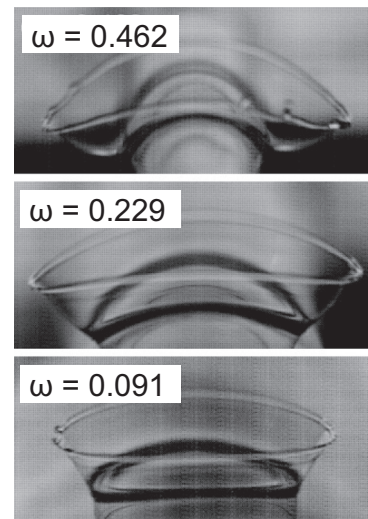


Fig. 9. Effects of wall curvature for drop–cylinder impact on crown shape for butanol with $We = 327\text{--}371$ and $h^* = 0.031\text{--}0.048$. Adapted from Liang et al. [100].

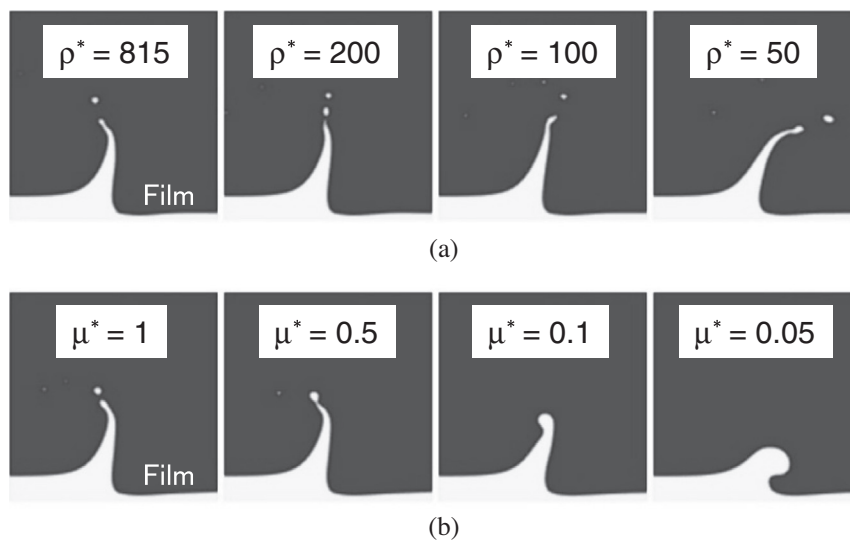


Fig. 8. Effects of gas density (a) and viscosity (b) on crown shape for water with $We = 693$ and $h^* = 0.3$. Adapted from Liang et al. [32].

eventually slides downward due to gravity. But by reducing ω (i.e., increasing the cylinder's diameter), the behavior of the liquid sheet gradually approaches that for drop impact on a flat film.

4.2. Crown evolution

4.2.1. Crown diameter

The main geometrical parameters of crown formation are crown diameter, D , height, H , angle, α , and thickness. Shown in the 2.0-ms image in Fig. 5 are the crown height and two different outer crown diameters, D_b and D_r , corresponding to the crown's base and top rim, respectively. Another diameter cited by some authors is the crown's inner diameter [54,91,102]. The height, H , is measured from the base to the rim, and angle, α , refers to the angle at the base; this angle changes away from the base because of the crown wall's curvature. Yarin and Weiss [27] recommended a theoretical square-root dependence of non-dimensional crown diameter, D^* , on non-dimensional time, τ ,

$$D^* = C(\tau - \tau_0)^n \quad n = 1/2, \quad (5)$$

where τ_0 corresponds to initial value corresponding to moment of impact. However, attempts to fit experimental data using Eq. (5) proved unsuccessful [102], which implies this relation is not applicable to all types of crown evolution. In fact, correlations by other researchers, which are listed in Table 2, prove that the value of exponent n in several situations is slightly less than the 1/2 value recommended by Yarin and Weiss. Additionally, Cossali et al. [54] reported that, while the coefficient C in Eq. (5) is independent of the film thickness, it is not constant but weakly dependent on impact velocity.

Liang et al. [65] investigated the dependence of crown size on drop Weber number, We , and Reynolds number, Re , by varying impact velocity and physical properties separately. They showed that the crown diameter is independent of We and Re , a conclusion shared by Rieber and Frohn [72], Josserand and Zaleski [104], and

Agbaglah and Deegan [105]. However, Fujimoto et al. [106] used numerical simulations to determine that surface tension plays a measurable role in reducing the development of the crown's liquid sheet.

Another parameter that influences crown diameter is non-dimensional film thickness, h^* . Some investigators suggest that crown diameter can be increased by reducing h^* because of the decreased energy dissipation and liquid mass [65,95]. However, theoretical studies [27,72] have shown that increasing h^* has an adverse effect on crown diameter. Cossali et al. [54] and Lee et al. [74] suggested that crown diameter is only weakly dependent on h^* . Ninomiya and Iwamoto [56] found that, for a milk drop, the crown's base diameter, D_b , increases while the rim diameter, D_r , gradually decreases as h^* is increased from 0.11 to 1.1, and the influence of h^* can be neglected for $h^* > 1.5$. On the other hand, Mukherjee and Abraham [86] concluded that crown diameter grows with increasing film thickness for thin films ($h^* < 0.25$), but decreases for thick films ($0.25 < h^* < 2$); the latter trend is caused by more of the impact drop's energy being absorbed by the thick film [86].

4.2.2. Crown height

The model by Roisman and Tropea [96] shows that non-dimensional crown height, $H^* = H/d_{drop}$, increases appreciably with increasing h^* . However, experiments by Cossali et al. [54] showed a strong dependence of crown height evolution on We but a very weak dependence on h^* , as shown in Fig. 10. They attributed the conflicting conclusions regarding the influence of h^* to the fact that the analytical model of Roisman and Tropea does not account for velocity component normal to the wall when varying the film thickness [54]. In studies by Davidson [103] and Šikalo and Ganić [15], the crown height achieved at a given instant increases with increasing h^* . Later, Mukherjee and Abraham [86] identified different crown height trends for very thin films, $h^* < 0.25$, versus those for thicker films, $h^* > 0.25$. Using an energy balance, Macklin and Metaxas

Table 2
Correlations of crown diameter.

Author(s)	Fluid(s)	Test conditions	Correlation(s)
Yarin and Weiss [27]	Ethanol or mixtures of ethanol, glycerol, and water	$d_{drop} = 70\text{--}340 \mu\text{m}$, v_{drop} up to 30 m/s	$D_r^* = \frac{2v_{drop}^{1/2}}{6^{1/4}\pi^{1/2}v_j^{3/8}d_{drop}^{1/4}}(\tau - \tau_0)^{1/2}$ simplified to $D_r^* = 2\left(\frac{2}{3h^*}\right)^{1/4}(\tau - \tau_0)^{1/2}$
Cossali et al. [54]	Distilled water	$d_{drop} = 3.82 \text{ mm} \pm 4\%$, $v_{drop} = 2.3\text{--}4.4 \text{ m/s}$, $h = 1.1\text{--}4.3 \text{ mm}$, $h^* = 0.29\text{--}1.13$	$D^* = C(\tau - \tau_0)^{0.43 \pm 0.03}$, $\tau_0 = 0\text{--}1.5$
Rieber and Frohn [72]	Water–air system, $\rho^* = 1000$, $\mu^* = 40$	$We = 250$, $Oh = 0.0014$, $h^* = 0.116$ $We = 598$, $Oh = 0.0014$, $h^* = 0.116$	$D_r^* = 2.44\tau^{0.406}$, $D_b^* = 2.116\tau^{0.459}$ $D_r^* = 2.30\tau^{0.441}$, $D_b^* = 2.130\tau^{0.444}$
Trujillo and Lee [95]	Ethanol	$d_{drop} = 3.4 \text{ mm}$, $v_{drop} = 1.3 \text{ m/s}$, $h^* = 0.25$	$D_r^* = C\tau^{1/2}$
Davidson [103]	Water	$We = 20\text{--}400$, $h^* = 0.1\text{--}0.5$	$D_b^* = C\tau^{1/2}$
Xie et al. [91]	Glycerol–water solution	$We = 2010$, $Oh = 0.0384$, $h^* = 0.5$	$D^* = 0.01826(\tau + 0.4)^{1/2}$ for crown's inner diameter
Guo et al. [80]	Water	$d_{drop} = 2 \text{ mm}$, $v_{drop} = 2.75\text{--}4.32 \text{ m/s}$, $h^* = 0.3\text{--}0.7$	$D_r^* = C\tau^n$, $n = 0.469, 0.447$ and 0.435 for $h^* = 0.3, 0.5$ and 0.7 , respectively

[107] derived a relation between maximum crown height, H_{\max}^* , and maximum diameter of the cavity, $D_{c-\max}^*$, beneath the crown,

$$H_{\max}^* = \frac{1 + 6 We^{-1} + 2 Fr^{-1} - 3 We^{-1} h^* D_{c-\max}^*}{6 We^{-1} D_{c-\max}^*}. \quad (6)$$

It should be emphasized that all parameters in the above equation were scaled by drop radius, $d_{\text{drop}}/2$, rather than drop diameter. Regarding the influence of liquid properties, high viscosity and high surface tension have been reported to inhibit crown height growth, with the crown dying out faster at higher viscosities [74,106].

Cossali et al. [54] concluded that non-dimensional maximum height, H_{\max}^* , and corresponding non-dimensional time, τ_{\max} , depend on impact velocity but are weakly dependent on film thickness. They recommended correlations for both H_{\max}^* and τ_{\max} of the form CWe^n , where $0.65 < n < 0.75$ [54]. On the other hand, Asadi and Passandideh-Fard [71] recommended the following correlations for the same parameters for $We = 296\text{--}1020$,

$$H_{\max}^* = 0.0025 We \quad (7a)$$

and

$$\tau_{\max} = 0.0037 We^{1.2}. \quad (7b)$$

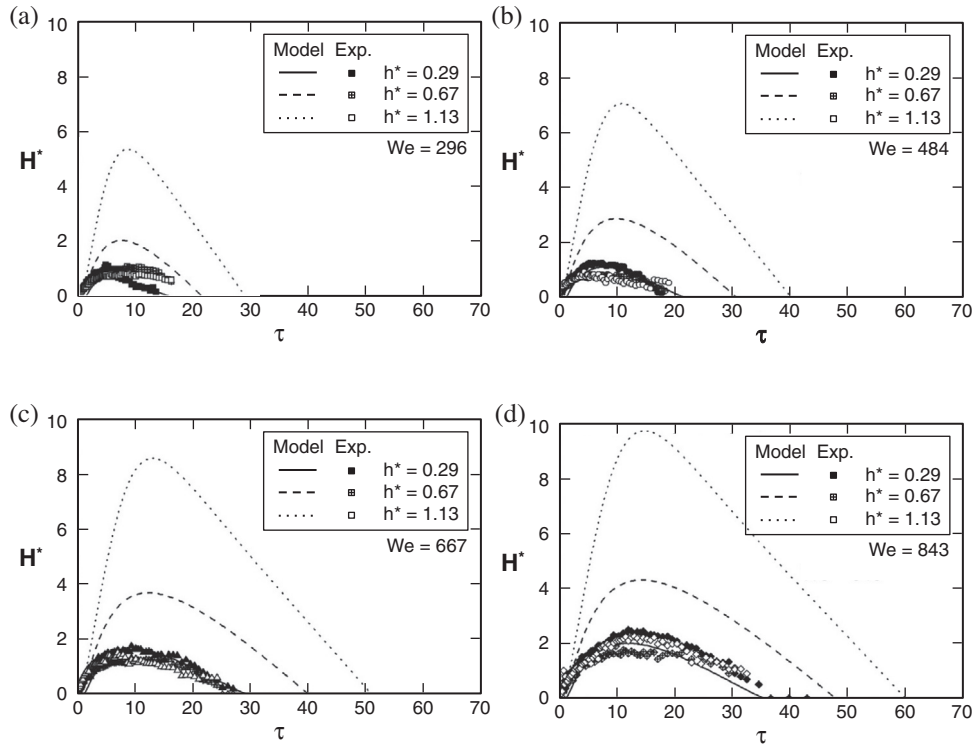


Fig. 10. Non-dimensional crown height evolution relative to non-dimensional time for different film thicknesses according to measurements of Cossali et al. [54] and theoretical predictions of Roisman and Tropea [96] for (a) $We = 296$, (b) $We = 484$, (c) $We = 667$, and (d) $We = 843$. Adapted from Cossali et al. [54].

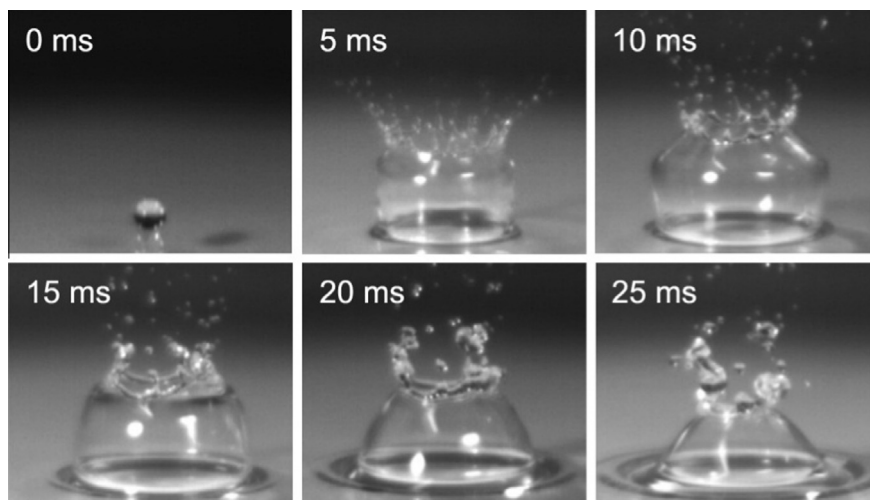


Fig. 11. Crown evolution of ethanol drop with narrow rim for $h^* = 0.3$ and $v_{\text{drop}} = 3.65$ m/s (Guo et al. [109]).

4.2.3. Crown angle

The theoretical model by Roisman and Tropea [96] resulted in the crown angle relation given by Eq. (4b). Unfortunately, this relation includes liquid velocity in the liquid film, which is difficult to determine. Wang and Chen [24] determined that the crown wall is almost perpendicular to the horizontal liquid film (*i.e.*, $\alpha = 90^\circ$) for $h^* = 0.5$. Later, Fedorchenko and Wang [108] noted that the crown angle is determined entirely by film thickness, independent of impact velocity or liquid properties. They concluded that, in the initial stages of crown emergence, $\alpha = 90^\circ$ for $h^* \geq 0.25$, but for very thin films with $h^* < 0.25$, the crown angle can be determined from

$$\cos \alpha = 1 - 4h^*. \quad (8)$$

4.2.4. Crown thickness

Several researchers reported the formation of crowns with narrow or closed rims [26,56,109] as shown in Fig. 11. It is believed that the formation of a closed rim crown, which tends to capture a large bubble, is strongly influenced by non-dimensional film thickness and impact velocity [110]. However, to the authors' knowledge, there is no published research addressing or predicting the angle of the top inclined rim for closed rim crowns as shown in the 10-ms image in Fig. 11.

The crown generated by drop impact on a film does not acquire uniform thickness, and determination of the detailed thickness is quite illusive. Using a light intensity technique, Cossali et al. [54] were able to obtain approximate measurements of this so-called normal thickness, defined as half the difference between the outer and inner crown diameters. Therefore, detailed temporal and spatial distributions of crown thickness can only be determined from numerical simulations [106], which reveal this thickness decreases with decreasing surface tension.

4.2.5. Cavity beneath the crown

Studies have shown that concentric capillary ripples travel along the cavity sidewall and change the shape of the cavity from hemispherical for deep pools and oblate for films to conical [91,111]. In the initial stages of cavity expansion, the cavity diameter follows closely the square-root time dependence predicted by Yarin and Weiss [27]. But, at later stages, the cavity evolution

deviates from this dependence because of capillary and gravitational effects [112].

Macklin and Metaxas [107] theoretically derived the following relation for maximum cavity radius by assuming a hemispherical cavity shape and neglecting kinetic energy of the target liquid,

$$\frac{D_{c-\max}^*}{2} = \left[Fr \left\{ 3.3 We^{-1} + (10.7 We^{-2} + 2.4 Fr^{-1} (1 + 2 Fr^{-1} + 6 We^{-1}))^{1/2} \right\} \right]^{1/2}. \quad (9)$$

Roisman and van Hinsberg [112] modeled the cavity growth theoretically using the kinematic discontinuity approach. Their model yielded the following relations for cavity radius and time required to reach maximum radius,

$$\frac{D_c^*}{2} = \sqrt{\beta \tau' - \left(\frac{2h^*}{We D_{c-\max}^*/2} + \frac{4}{We} + \frac{h^{*2}}{Fr} \right) \frac{\tau'^2}{h^*}} \quad (10a)$$

and

$$\tau_{c-\max} = \frac{\beta h^*}{2} \left(\frac{2h^*}{We D_{c-\max}^*/2} + \frac{4}{We} + \frac{h^{*2}}{Fr} \right)^{-1}, \quad (10b)$$

where β and τ' are functions of only the initial film thickness for $0.5 < h^* < 2$, and given, respectively, by

$$\beta = 0.62 h^{*-0.33} \quad (11a)$$

and

$$\tau' = \tau - 0.8 h^{*1.7}. \quad (11b)$$

Assuming a hemispherical cavity shape, Berberović et al. [111] showed analytically that initial growth of the cavity for $\tau > 2$ follows the relation

$$\frac{D_c^*}{2} = 2^{-4/5} (5\tau - 6)^{2/5}, \quad (12)$$

which showed good agreement with experimental data. They also derived the following relation for residual film thickness,

$$h_{res}^* = C Re^{-2/5}, \quad (13)$$

where the coefficient C is a function of h^* , We and Fr . Later, van Hinsberg et al. [113] recommended the following approximate scaling relation for C ,

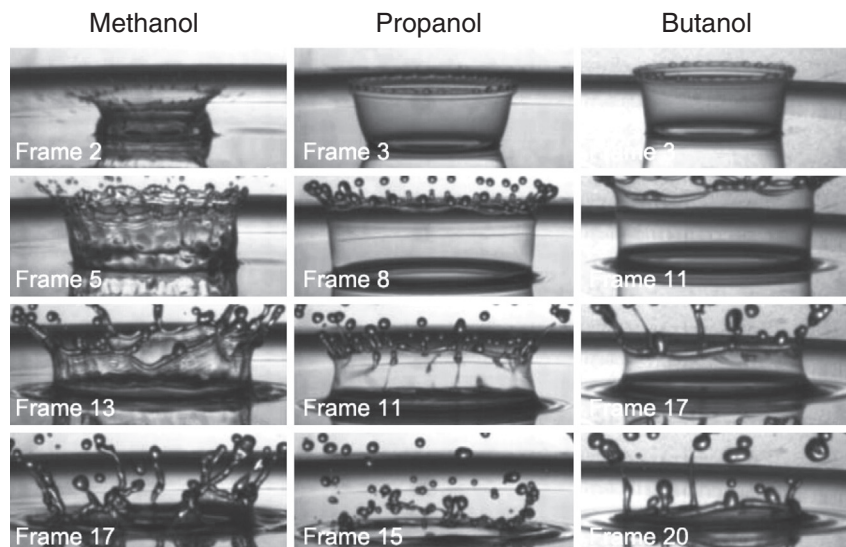


Fig. 12. Prompt splashing in methanol drop impact, and delayed splashing in propanol and butanol drop impact for $d_{drop} = 2$ mm, $h^* = 0.1$ and $v_{drop} = 3.15$ m/s. Adapted from Vander Wal et al. [23].

$$C = 0.098 h^{*4.0413} + 0.79. \quad (14)$$

This equation agrees well with experimental measurements for $h^* \leq 1.5$, but shows some deviation around $h^* = 2.0$, where the effect of film thickness becomes much weaker and the initial impact resembles that with a deep liquid pool. Hillen et al. [114] reported that static film thickness has stronger influence on minimum liquid volume under the cavity than the initial drop parameters, but that the latter parameters do influence cavity lifetime. Kuhlman et al. [115] measured the time dependence of liquid volume beneath the cavity, and determined that this volume is maintained at 30–35% of the drop volume over much of the cavity lifetime. They also measured the thickness of the residual film using a non-contact optical thickness sensor, and determined that this thickness decreases away from the cavity centerline to the immediate vicinity of the inner crown wall.

4.3. Splashing phenomena

4.3.1. Splashing types

Splashing takes place at relatively high drop impact velocities, and is accompanied by the production of tiny drops, named *secondary droplets* [19,23,25]. This phenomenon is crucial to atomization, but is often detrimental in coating processes, such as ink jet printing and pesticide delivery [12]. Cossali et al. [25] distinguished two types of splashing: *prompt splashing* and *delayed splashing*. Prompt splashing is associated with droplet ejection from the crown's rim while the crown is still growing, as shown for methanol drop impact in Fig. 12. On the other hand, delayed splashing occurs near or after the crown reaches maximum height as shown for propanol and butanol in Fig. 12, and is associated with breakup of the crown's rim. Additionally, delayed splashing can often be observed in the latter stages of prompt splashing as shown for methanol in Fig. 12.

Overall, the splashing type can be influenced by viscosity and surface tension. Experiments by Cossali et al. [25], Motzkus et al. [116], and Liang et al. [117] reveal that prompt splashing takes place in low Oh (i.e., low viscosity) situations, while high Oh (high viscosity) systems result in delayed splashing, and secondary droplets in prompt splashing are much smaller than those in delayed splashing [25,118]. Vander Wal et al. [23] conducted extensive experiments with different liquids to assess the influence of liquid properties on splashing. They reported that high surface tension inhibits splashing regardless whether the target surface is dry or covered with a thin liquid film. The same conclusion was drawn later by Liang et al. [117]. However, viscosity has different influences for a dry versus wet surface, promoting splashing on the dry surface but resisting splashing for droplet impact on a thin film [23].

Another factor that may influence the splashing is properties of the surrounding gas. Liang et al. [32] concluded that increasing gas viscosity serves to suppress splashing, but gas density has no influence on splashing. The latter conclusion was also confirmed in experiments by Zhang et al. [119]. Xu et al. [120,121] and Driscoll and Nagel [122] demonstrated that splashing on a solid surface can be completely suppressed by decreasing pressure of the surrounding gas; similar gas pressure effects may be expected for impact on a thin film.

4.3.2. Splashing mechanisms

A key method to investigating the splashing mechanism is to determine the splashing threshold, above which secondary droplets begin to form. This threshold is highly dependent on surface tension and is, therefore, expressed in terms of either We alone, or We in combination with other parameters. For impact on an inclined wetted surface or moving liquid film, splashing is

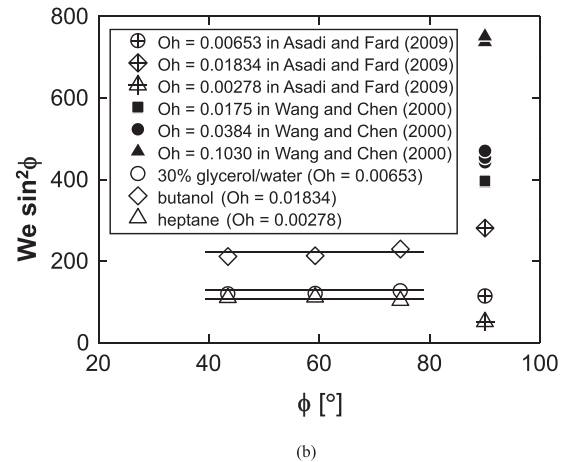
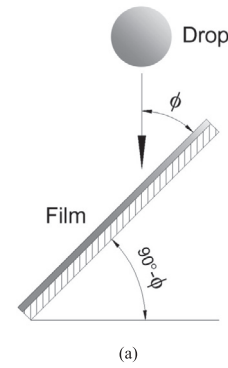


Fig. 13. (a) Schematic of drop impact on inclined wetted wall, and (b) variation of modified Weber number for splashing threshold with impact angle for different values of Oh . Adapted from Liang et al. [117].

asymmetric and impact angle, ϕ , must be incorporated in the thresholds [39,123]. Liang et al. [117] and Šikalo et al. [124] suggested that using normal Weber number, $We \sin^2 \phi$, to account for impact angle yields good agreement with normal splashing on a horizontal film. Studies reveal that the threshold We is influenced by both viscosity and film thickness. Fig. 13 shows that the influence of viscosity is reflected in the threshold We increasing with increasing Oh [24,25,71,125]. However, there is disagreement concerning the influence of film thickness. Cossali et al. [25] pointed out that the threshold We generally increases with increasing h^* , and Rioboo et al. [93] drew the same conclusion even for very thin films with $h^* = 0.02$ – 0.04 . However, other investigators suggested the threshold We is independent of h^* for thin films with $h^* < 0.1$ [24,71,126].

Given that both surface tension and viscosity have a strong influence on splashing thresholds, even for low viscosity liquids [93], use of We alone is insufficient to describe the threshold. A preferable method is to use K -type correlations combining drop inertia with surface tension force (We), viscous force (Oh or Re), and film thickness (h^*). Table 3 shows several correlations that are based on this method. Notice that, while the majority of correlations are based solely on We and Oh , a few [54,116,127,128] also account for h^* .

Motzkus et al. [116] used their experimental data to assess the predictive accuracy of some of the correlations in Table 3. Their comparisons of data to correlations are shown in Fig. 14(a)–(d) in the form of threshold We versus h^* for $Oh = 2.4 \times 10^{-3}$, 6.8×10^{-3} , 9.5×10^{-3} and 1.5×10^{-2} , respectively. The data are segregated according to delayed splashing (D), prompt splashing (P), and coalescence (C). For $Oh = 2.4 \times 10^{-3}$, Fig. 14(a), the

Table 3
Correlations for critical K required to initiate splashing into small droplets.

Author(s)	Fluids	Test conditions	Correlation(s)
Walzel [129]	Glycerol–water mixtures	$h^* = 0.1$	$K = We Oh^{-0.4} = 2500$
Yarin and Weiss [27]	Ethanol, ethanol–glycerol–water mixtures	$d_{drop} = 70\text{--}340 \mu\text{m}$, v_{drop} up to 30 m/s	$v_{drop} = \left(\frac{\sigma}{\rho_f}\right)^{1/4} v_f^{1/8} f^{3/8}$ simplified to $K = We Oh^{-0.4} = 2400$
Cossali et al. [54]	Water, glycerol–water mixtures	$d_{drop} = 3.07 \pm 0.07\text{--}$ $3.51 \pm 0.06 \text{ mm}$, $We = 2 \times 10^2\text{--}1.6 \times 10^3$, $h^* = 0.1\text{--}1$, $Oh > 7 \times 10^{-3}$	$K = We Oh^{-0.4} = 2100 + 5880h^{1.44}$
Marengo and Tropea [127]	Water $\mu_f = 50 \text{ mPa s}$	– $Oh > 0.01$	$K = We Oh^{-0.4} = 2074 + 870h^{0.23}$ $K = We Oh^{-0.4} = 2164 + 7560h^{1.78}$
Rioboo et al. [93]	Glycerol–water mixtures, hexadecane, PDMS ₅ , PDMS ₁₀	$We = 28\text{--}890$, $h^* > 0.06$, $Oh = 1.14 \times 10^{-2}\text{--}5.48 \times 10^{-2}$	$K = We Oh^{-0.4} = 2100$
Okawa et al. [55]	Water	$We = 2.5\text{--}980$, $h^* = 0.4\text{--}68$, $Oh = 1.5 \times 10^{-3}\text{--}7 \times 10^{-3}$	$K = We Oh^{-0.4} = 2100$
Vander Wal et al. [13]	Heptane, nonane, decane, dodecane, tetradecane, hexadecane, deionized water, 30% glycerol/water, methanol, ethanol, n-propanol and butanol	$Re = 5 \times 10^2\text{--}5 \times 10^3$, $Oh = 10^{-3}\text{--}2.2 \times 10^{-3}$	$K = Oh Re^{1.17} = 63$
Huang and Zhang [128]	Water, oil	$h^* = 0.1\text{--}1$, $\rho_f = 854\text{--}998 \text{ kg/m}^3$, $\mu_f = 1\text{--}22.5 \text{ mPa s}$, $\sigma = 0.029\text{--}0.072 \text{ N/m}$	$K = (We Re)^{0.25} = 25 + 7h^{1.44}$
Motzkus et al. [116]	Water, glycerol–water mixtures	$We = 62\text{--}1754$, $h^* = 0.3\text{--}1$, $Oh = 2 \times 10^{-3}\text{--}1.5 \times 10^{-2}$	$K = We Oh^{-0.4} = 2100 + 2000h^{1.44}$
Gao and Li [101]	Water, glycerin–water mixtures	$h^* v_{lim}^2 = 0.05\text{--}0.18$, $\mu_f = 1\text{--}46.47 \text{ mPa s}$, $\sigma = 0.0657\text{--}0.0714 \text{ N/m}$	$K = We Re^{0.5} = 3378(1 + h^* v_{lim}^2)^{-1} (1 + h^* v_{lim}^2)^{-0.5}$

coalescence/prompt splashing ($C\text{--}P$) limit is independent of h^* , and well predicted for $0.5 < h^* < 1$ by Vander Wal et al. [13] and Okawa et al. [54], however, h^* does appear to influence the prompt/delayed splashing ($P\text{--}D$) limit. As Oh is increased to 6.8×10^{-3} , Fig. 14(b), the $C\text{--}P$ limit begins to show a dependence on h^* for $0.3 < h^* < 6$, and the $P\text{--}D$ and $C\text{--}P$ limits are predicted well by Cossali et al. [54] and Motzkus et al. [116], respectively. Increasing Oh further to 9.5×10^{-3} , Fig. 14(c), and 1.5×10^{-2} , Fig. 14(d), which are associated with high viscosity liquids, increases the dependence on h^* , with the $C\text{--}P$ limit predicted by the correlation of Motzkus et al., albeit with less accuracy, while the $P\text{--}D$ limit is incorrectly predicted by the Cossali et al. correlation. These deviations between data and correlations might be related to the fact that these correlations are tested beyond their validation ranges.

Many authors determined that splashing is greatly influenced by gas pressure and gas properties [32,40,119–122,130–133]. This implies that conventional scaling approaches based solely on We , Re and Oh are insufficient to predict the splashing thresholds. Thus, more accurate scaling models are required to account for the gas effects.

4.3.3. Jets and secondary droplets

According to Deegan et al. [31], there are at least three sources of secondary droplets based each on a different source of instability: (i) prompt instability of the ejecta sheet that occurs immediately upon impact and produces very small droplets, (ii) rim instability of the ejecta sheet that produces medium sized droplets, and (iii) rim instability of the crown sheet that produces jets followed by large droplets. Fig. 15 shows the third type of instability. The number of jets along the rim decreases with time for $0 < \tau < 8$,

before stabilizing to about 10, independent of film thickness or impact velocity [27,54]. The length of jets, which is influenced by the crown thickness, increases with time [54].

Using theoretical premises, Engel [135] proposed that only about 5% of the impinging drop's kinetic energy is carried away by the secondary droplets. They also found that the total volume of secondary droplets may reach 2–4 times the volume of the impinging drop. Okawa et al. [123] reported that when impingement angle is higher than 40° , an increase in the impingement angle leads to a substantial increase in the total mass of secondary drops. Cossali et al. [25] concluded from their experiments that, for high viscosity liquids, secondary droplets detach only after full development of the crown, whereas the secondary droplets in low viscosity liquids may begin to detach from the initial jets. Later, Vander Wal et al. [23] and Davidson [103] reported that increasing surface tension decreases the number of secondary droplets while increasing their size during the splashing. Vander Wal et al. and Motzkus et al. [26] found that increasing liquid viscosity has the same effect on the number and size of secondary droplets as surface tension. Motzkus et al. also reported that increases in impact velocity and diameter of the drop increase the number of secondary droplets in the 2–50 μm size range, and the smallest droplets are created during the early stages of the crown development. Quantitative works by Gregory et al. [136] and Hobbs and Osheroff [137] showed that the number of secondary droplets increases with decreasing film thickness. Hobbs and Osheroff also concluded the number of secondary droplets increases with increasing maximum height of the jet [137]. Allen [138] found that the angle at which the secondary droplets are ejected depends on h^* . According to Cossali

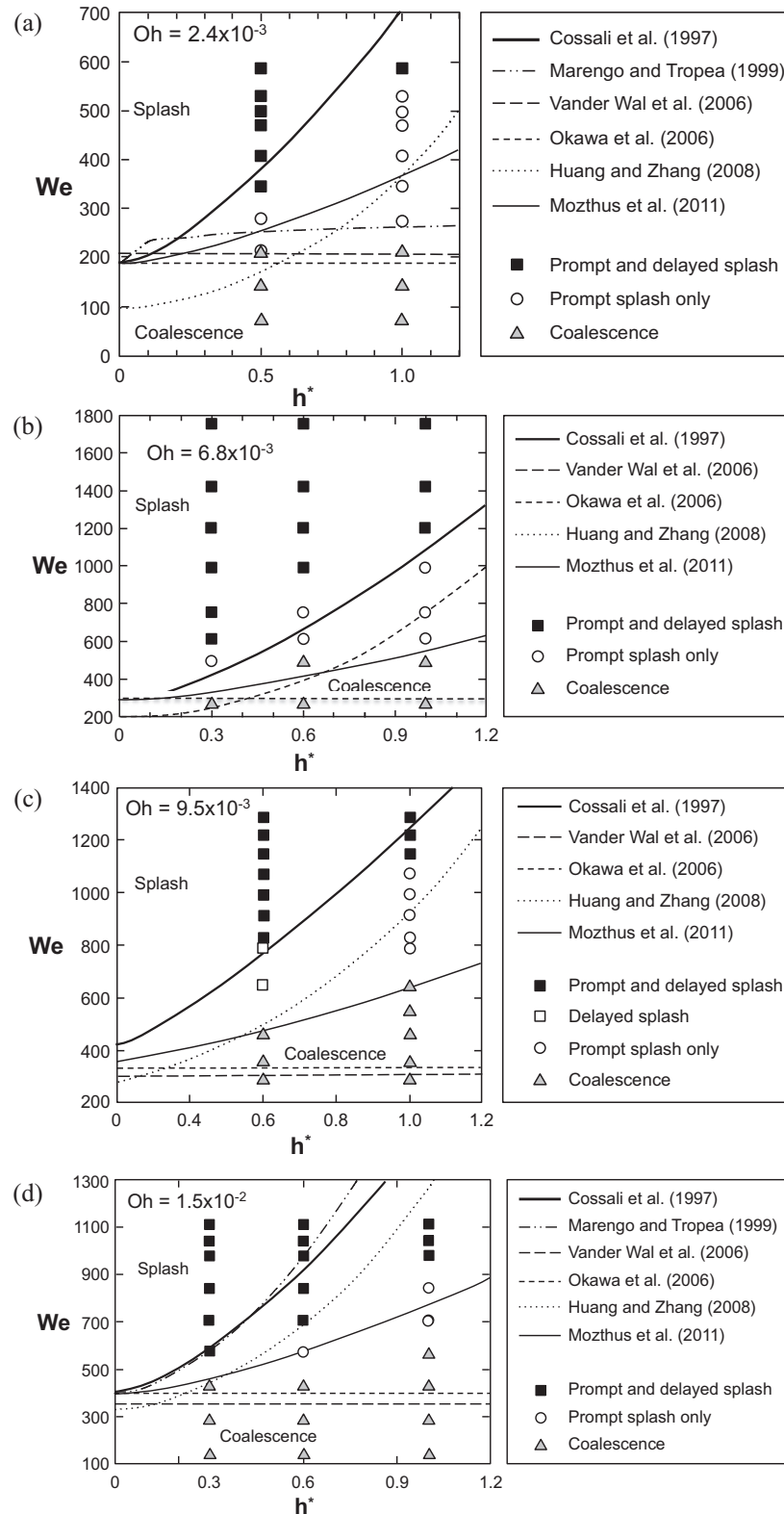


Fig. 14. Comparison of different splashing thresholds for (a) $Oh = 2.4 \times 10^{-3}$, (b) $Oh = 6.8 \times 10^{-3}$, (c) $Oh = 9.5 \times 10^{-3}$ and (d) $Oh = 1.5 \times 10^{-2}$. Adapted from Motzkus et al. [116].

et al. [54], the maximum number of droplets is achieved when the crown evolution begins ($\tau = 1-3$), independent of experimental conditions. Table 4 provided correlations for the number of secondary droplets.

To date, the dominant view for the mechanism of production of secondary droplets is Rayleigh-Plateau [139] capillary instability, which causes cylindrical jets to break into droplets, driven by surface tension [34]. Rieber and Frohn [72] found support of the

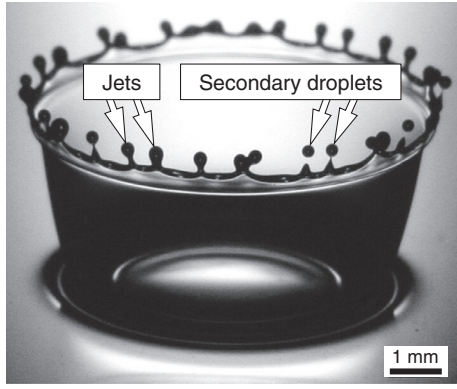


Fig. 15. Jets and secondary droplets in splashing of silicone oil drop with $Re = 966$, $We = 874$ and $h^* = 0.2$. Adapted from Zhang et al. [134].

Rayleigh-Plateau mechanism by employing large initial perturbations in their 3D simulations. Fullana and Zaleski [140] argued that the growing cylindrical rim does not break into droplets for mod-

erate wavelengths. Additional support of the Rayleigh-Plateau instability as the leading mechanism for production of secondary droplets comes from recent studies by Bremond and Villermaux [141] and Lagubeau et al. [142]. Deegan et al. [143] and Zhang et al. [134] verified the Rayleigh-Plateau mechanism by measuring the spectrum of small-amplitude perturbations growing on the rim.

Yarin [19] and Yarin and Weiss [27], however, concluded that the number of jets observed in experiments is inconsistent with the Rayleigh-Plateau mechanism. They suggested the main cause is a nonlinear amplification mechanism, which they based on the observation that the free rim always propagates normal to the crown sheet. According to Taylor [144], a two-dimensional liquid sheet is rearranged by surface tension into a free rim along the sheet's edge. Yarin [145] suggested that a rim on any liquid film inevitably forms cusps, and these cusps become sites where nearly one-dimensional jets are squeezed out, thereafter undergoing capillary breakup. This mechanism is shown schematically in Fig. 16 (a) and (b). Roisman et al. [52] proposed that transverse instability of the rim leads to cusp formation and jetting, and rim deceleration can accentuate the rim's instability.

Table 4
Correlations for number of secondary droplets.

Authors	Fluids	Test conditions	Correlation
Yarin and Weiss [27]	Ethanol, mixtures of ethanol, glycerol and water	$d_{drop} = 70\text{--}340 \mu\text{m}$, v_{drop} up to 30 m/s	$N = \frac{15\pi D^2}{4.5}$
Cossali et al. [54]	Water	$d_{drop} = 3.82 \pm 4\%$ mm, $v_{drop} = 2.3\text{--}4.4$ m/s, $h = 1.1\text{--}4.3$ mm, $h^* = 0.29\text{--}1.13$	$N = C\tau^n$, n increases with increasing We
Okawa et al. [55]	Water	$We = 2.5\text{--}980$, $Oh = 1.5 \times 10^{-3}\text{--}8.4 \times 10^{-3}$, $h^* = 0.43\text{--}68$	$N = 7.84 \times 10^{-6} K^{1.8} h^{*-0.3}$, where $K = We Oh^{-0.4}$

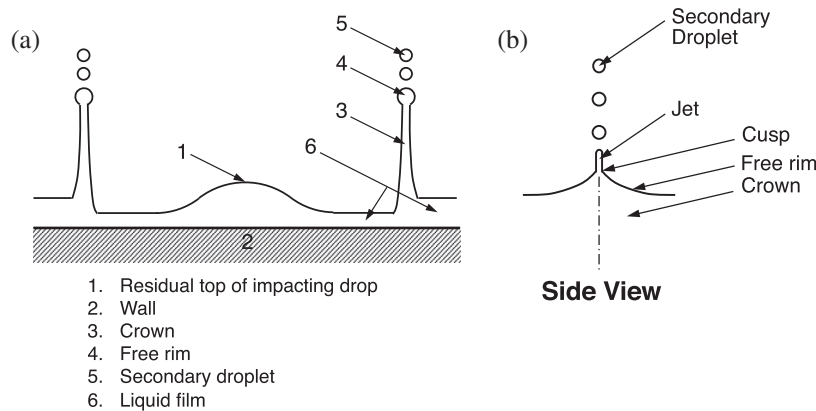


Fig. 16. Splashing mechanism of nonlinear amplification according to Yarin [19]: (a) schematic of splashing mechanism, (b) free rim and secondary droplets formation.

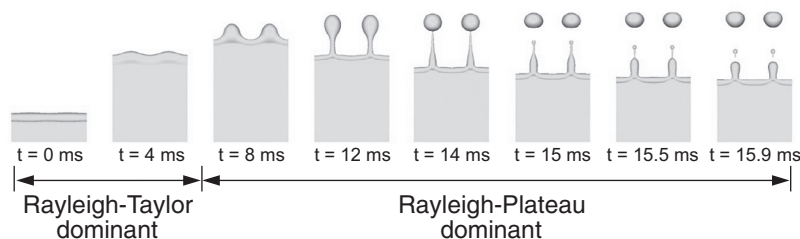


Fig. 17. Mechanism of liquid jet formation and rim breakup from a 3D sheet of water with $Oh = 0.5$ and $Re = 10$. Adapted from Agbaglah et al. [151].

Mechanisms other than Rayleigh-Plateau and nonlinear amplification have also been proposed, including combinations of different types of instabilities. Roisman et al. [52,146,147] investigated the linear stability of a receding liquid sheet and concluded that the liquid rim is subject to both Rayleigh-Plateau and Rayleigh-Taylor instabilities. And, while Gueyffier and Zaleski [148] evoked the Richtmyer-Meshkov instability, Krechetnikov and Homsy [149] suggested a combination of the Richtmyer-Meshkov and Rayleigh-Taylor instabilities. The Richtmyer-Meshkov instability arises when a shock wave interacts with an interface separating two different fluids [150], and combines compressibility effects with hydrodynamic instability. According to the Krechetnikov and Homsy hypothesis, liquid along the crown's rim is initially impulsively accelerated into the air and is therefore Richtmyer-Meshkov unstable, and associated with a particular range of wavelengths that dictates the number of jets emanating from the rim. Shortly afterwards, when the interface begins to decelerate, the Rayleigh-Taylor instability is induced in the individual jets, and amplified to produce breakup of the secondary droplets. As illustrated in Fig. 17, Agbaglah et al. [151] and Krechetnikov [152] observed that rim instability is driven both by the Rayleigh-Taylor mechanism, because of initial rim acceleration, and the Rayleigh-Plateau mechanism, where the Rayleigh-Taylor instability is dominant at short times and the Rayleigh-Plateau becomes relevant at larger times when the rim begins to generate jets [105,151]. Thoroddsen et al. [153] proposed yet another mechanism, suggesting that when a viscous drop impacts a thin low-viscosity liquid film with significantly lower surface tension than the drop liquid, splashing from the crown breakup is promoted mainly by Marangoni-driven flow [153].

Overall, the mechanism governing the production of secondary droplets remains an open question. The disagreements among investigators point to a need for more comprehensive experiments involving broad ranges of operating parameters and fluid properties to identify truly dominant mechanisms.

5. Ejecta sheet, low-velocity impact and multi-drop impact

5.1. Ejecta sheet

When the liquid drop impacts a liquid film, it ejects a thin liquid sheet – ejecta sheet – from the drop-film neck region. This sheet, which is formed during the earliest stages (first milliseconds) of the impact, is ejected horizontally at high speed, evolving into a variety of intriguing shapes [49]. The ejecta sheet was first reported by Weiss and Yarin [46], in their inviscid flow simulations using the BIM method. Subsequently, Davidson [103] confirmed the existence of the ejecta sheet by employing a more accurate BIM discretization technique. Thoroddsen [49] provided the first photographic records of this phenomenon as shown in Fig. 18(a). Howison et al. [154] analyzed the ejecta sheet formation using the theoretical asymptotic method. Josserand and Zaleski [104] reported that viscosity plays a major role in influencing liquid motion in the neck region, and dictates the width of the ejecta sheet that ultimately develops into a crown. Thereafter, surface tension serves to either allow or prevent the formation of the ejecta sheet; the latter occurs when high surface tension causes the leading edge of the ejecta sheet to be pulled back and forms the crown's rim as it folds backwards [105].

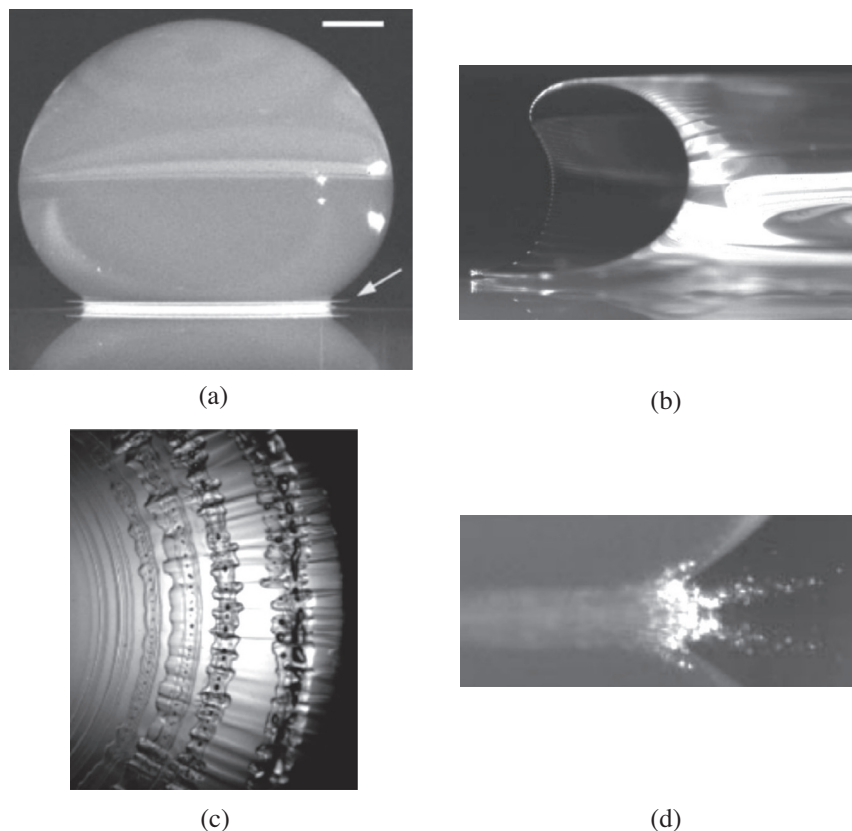


Fig. 18. (a) Initial formation of ejecta sheet in mixture of water and glycerin with $We = 4170$ and $Re = 1080$. (b) Ejecta sheet coming into a crown in mixture of water and glycerin with $We = 3340$, $Re = 770$ and $h^* = 0.48$. (c) Formation of bubble rings beneath ejecta sheet during a water drop impact on a shallow pool of ethanol with $We = 532$ and $Re = 13,300$. (d) Breaking of ejecta sheet in water with $We = 1800$ and $Re = 29,000$. (a), (b) and (d) are adapted from Thoroddsen [49], and (c) from Thoraval et al. [155].

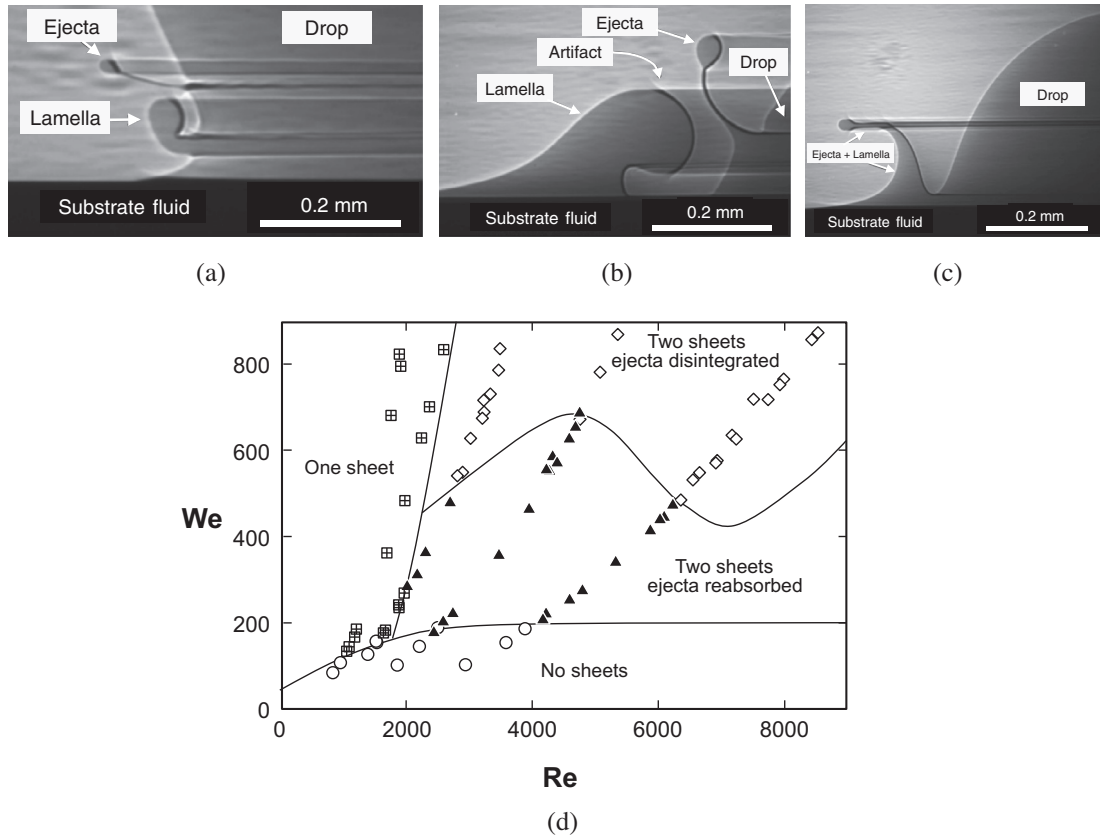


Fig. 19. Distinguishing ejecta and lamella for silicone oil with (a) $We = 396$ and $Re = 5703$, (b) $We = 324$ and $Re = 2191$, and (c) $We = 451$ and $Re = 710$. (d) Number of sheets resulting from drop impact. Adapted from Zhang et al. [48].

Table 5
Correlations for contact length.

Authors	Test conditions	Correlation
Josserand and Zaleski [104]	$h^* = 0.15$, $We = 8000$, $Re = 40-1000$	$r_e = 1.1 \sqrt{d_{drop} v_{drop} t}$
Coppola et al. [68]	$h^* = 0.1$, $We = 8000$, $Re = 387-5000$	$r_e = 1.476 \sqrt{d_{drop} v_{drop} t}$
Zhang et al. [48]	$h^* > 5$, $We = 117-798$, $Re = 710-8019$	$r_e = \sqrt{d_{drop} v_{drop} t}$
Agbaglah and Deegan [105]	$h^* = 0.2-5$, $We = 200-1000$, $Re = 500-4000$	$\frac{r_e}{d_{drop}} = \frac{13}{We} \tau + \frac{0.35}{We^{0.4} Re^{0.3}}$

Weiss and Yarin [46] and Deegan et al. [31] summarized the evolution of the ejecta sheet as follows. (i) The ejecta sheet becomes the leading edge of the crown sheet, as the latter grows underneath the former, as shown in Fig. 18(b). (ii) The ejecta sheet collides with the liquid film to produce bubble rings as shown in Fig. 18(c). (iii) The ejecta sheet breaks up immediately for prompt splashing conditions as shown in Fig. 18(d). Condition (iii) may lead to additional irregularity in the crown sheet and kickstart crown rim instability. In Fig. 18(b), the leading section of the ejecta sheet is shown bending down to meet the surface of the liquid film or pool. When the sheet touches the liquid below, it ruptures and sends off micro-droplets by a ‘slingshot’ mechanism [2]. In Fig. 18 (c), bubble rings are formed, which then break up into many tiny bubbles. An interesting von Kármán vortex street has been observed emerging in the bubble rings region [50,155–157].

However, most investigators do not distinguish between the ejecta and the lamella. As described above, the ejecta sheet is formed almost immediately (within 100 μs) upon impact, while the lamella is a slower sheet that emerges after the ejecta, typically 500–1000 μs after impact. Zhang et al. [48] dispelled the ambiguity concerning the two sheets by providing definitive evidence of both from experiments using an X-ray technique. Shown in Fig. 19 (a) and (b) are a thin ejecta sheet and a thicker lamella sheet. Fig. 19(c) shows the ejecta and lamella sheets combining into a single sheet. Fig. 19(d) shows a $We-Re$ regime diagram indicating the number and type of sheets resulting from the drop impact. Recently, Agbaglah and Deegan [105] found similar evidence of the two sheets from simulations. As indicated above, the ejecta sheet becomes the leading edge of the crown at low Re , but breaks up in the form of prompt random splashing at high Re [31,46]. However, there is a lack of understanding of the earliest stages of contact, including initial formation of the ejecta sheet [158], as well as the transition between the more ordered transition of the ejecta into the leading edge of the crown, and the more random ejecta splashing. Some of these issues were addressed in a follow-up study by Zhang et al. [119], who identified a third type of sheet (secondary ejecta) distinct from the ejecta or the lamella, that produces droplets with a size intermediate to those from the ejecta and the lamella. This, of course, adds further complexity to the depiction of events immediately following the droplet impact.

The thresholds for ejecta formation, and the ejecta’s speed, emergence time and position are four important parameters for quantitative characterization of the ejecta. Weiss and Yarin [46] indicated that the ejecta occurs at $We = 40$, but simulations by Davidson [103] point to a much higher value of $We = 200$, which

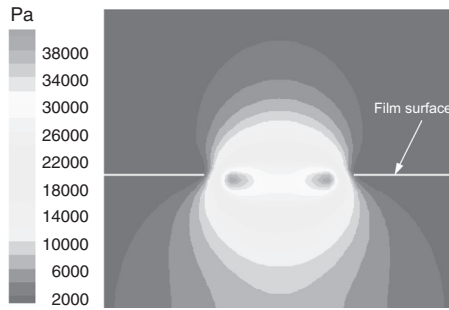


Fig. 20. Pressure distribution for water with $We = 667$, $Re = 13,676$, and $h^* = 0.67$ at $t = 0.25$ ms. Adapted from Liang et al. [65].

is close to value of $We = 180$ obtained experimentally by Zhang et al. [48].

According to Thoroddsen [49,104] and Josserand and Zaleski [49,104], the speed, v_e , of the intact ejecta decreases with increasing viscosity according to $v_e \sim \nu_f^{-1/2}$, and is much higher (over 10 times) than the impact velocity [49,104]. Josserand and Zaleski related the ejecta speed to impact velocity according to

$$v_e = Re^{0.5} v_{drop}. \quad (15)$$

Thoroddsen [49,104] and Coppola et al. [68] recommended an alternative velocity expression of the form $v_e \sim \nu_f^{-1/2} v_{drop}^{1.5}$. However, experiments by Zhang et al. [48] suggest that the ejecta speed depends more strongly on impact velocity, $v_e \sim \nu_f^{-1/4} v_{drop}^{1.8}$.

For the ejecta emergence time, t_e , which is measured from the moment of impact, Zhang et al. [48] found that $t_e \sim \nu_f^{1/2} / v_{drop}^{2.6}$, while Coppola et al. [68] stated that their data do not follow a power law relative to time.

The ejecta position is defined in terms of contact length, r_e , which is the distance from the drop centerline to the neck. Table 5 provides a summary of correlations for r_e .

Other interesting aspects of the ejecta sheet can be inferred from pressure distribution shortly after impact. Most significantly, as shown in Fig. 20, a pressure peak is observed along the impact neck [65,68,94,104], and the maximum pressure is given by [104]

$$P_{max} = \rho_f v_{drop}^2 \tau^{0.5}. \quad (16)$$

Liang et al. [94] pointed out that the high pressure in the neck contributes to the generation of the ejecta sheet, the effect of which gradually abates with impact evolution as the ejecta sheet develops into the leading edge of the crown, aided by radial flow in the liquid film.

5.2. Low-velocity impact

Three important phenomena associated with low-velocity impact are spreading, coalescence and rebound. Drop spreading is more commonly investigated in studies of drop impact on a solid dry wall [83,159–163], mainly for the purpose of describing

wetting or cooling phenomena. *Deposition* is a term similar to spreading, except that it refers to relatively lower velocities, where the impact fails to generate capillary waves [68]. *Coalescence* is commonly encountered in drop impact on a liquid pool at low velocity [11,78,79,164–167]. In experiments by Liang et al. [117], a liquid drop impacting a very thin film (less than 100 μm) below 0.74 m/s was observed to avoid coalescing directly with film's liquid. Instead, the drop spread over the film forming its own liquid film. About 1–2 min later, liquid from the newly formed film coalesced completely with the original film. But if the film is thick enough, the impact results in early coalescence between the drop's liquid and the original film.

Broad spreading of the drop's liquid is desired in some applications such as ink jet printing [168]. Several authors investigated the drop's spreading scale (span) in the initial stages following low velocity impact on a horizontal liquid film [68,69,103,104]. Chowdhury et al. [169] reported the spreading and recoil of surfactant-containing, low velocity water drops on various alcohol films with $h = 72$ μm supported on glass slides. They found that the concentration of surfactant in the drop plays a crucial role in the spreading and recoil time of the drop, with higher surfactant concentrations hastening both the spread and recoil. Liang et al. [117] and Šikalo et al. [124] examined low velocity drop impact on an inclined target covered by a thin film whose thickness is determined by impact angle, ϕ , and liquid type as shown in Fig. 13(a). Šikalo et al. speculated that the outcomes of inclined low velocity impact on a liquid film are similar to those on a dry surface. But experiments by Liang et al. [117] showed that the two are quite different, noting that the initial front and back spreading velocities increase with increasing impact velocity and impact angle. They explained the unexpected influence of impact angle on the front spreading velocity by the combined effects of viscous dissipation and tangential component of the impact velocity. Liang et al. [170] also showed that the front spreading span can be increased by increasing impact velocity or reducing impact angle, whereas the back spreading span is weakly dependent on impact velocity but increases with decreasing impact angle.

Drop rebound is closely associated with low impact We . Liang et al. [171,172] investigated drop rebound on wetted cylindrical and spherical surfaces; images of impact on a cylindrical surface are shown in Fig. 21. They suggested that the critical We for rebound must lie between upper and lower limits, rather than be smaller than a specific value. An impact We above the upper limit would cause the air layer between the drop and wetted surface to be damaged by shear upon impact, so the drop begins to spread on the wetted surface. On the other hand, an impact We below the lower limit may not possess sufficient kinetic energy to bounce off the wetted surface. Unfortunately, they were not able to accurately determine the lower limit because of large errors associated with very low velocity measurements. The upper limit of about $We = 9.2$ was found to be insensitive to surface curvature for low curvatures below $\omega = 0.5$, but decreases with increasing curvature for $\omega > 0.5$. For We values exceeding the upper limit, the drop was observed to spread on very thin films, and the spreading span for wetted cylinders can be expressed as a power law of dimensionless time τ , according to

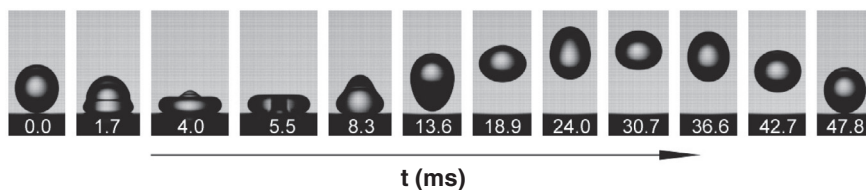


Fig. 21. Drop rebound on a wetted cylinder for butanol with $We = 4$ and $\omega = 0.091$. Adapted from Liang et al. [171].

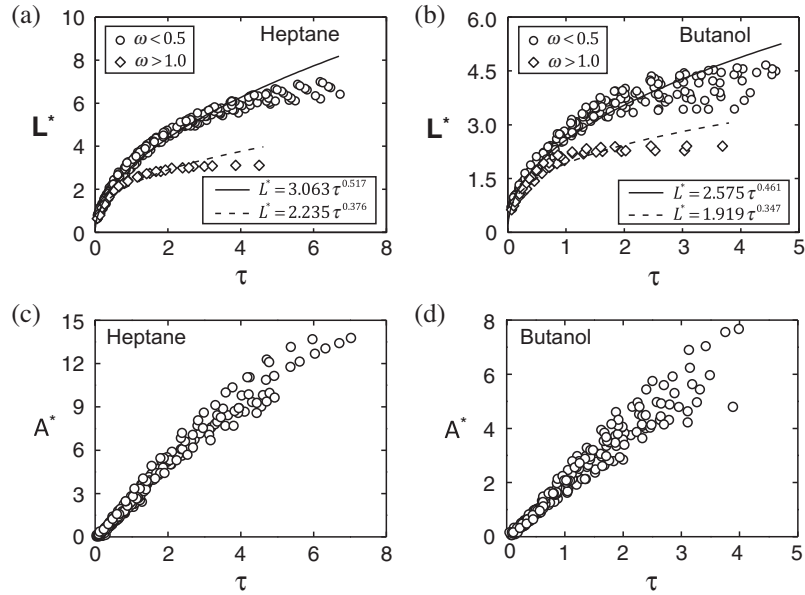


Fig. 22. (a) Heptane drop spreading on wetted cylinder. (b) Butanol drop spreading on wetted cylinder. (c) Heptane drop spreading on wetted sphere. (d) Butanol drop spreading on wetted sphere. (a) and (b) are adapted from Liang et al. [171], and (c) and (d) from Liang et al. [173].

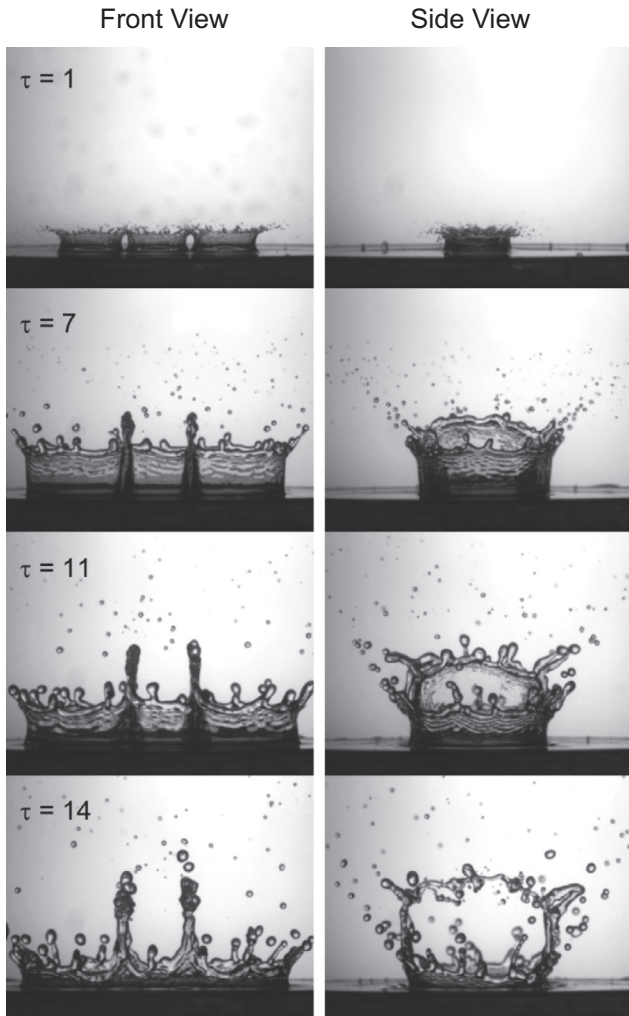


Fig. 23. Evolution of interfacial behavior for three adjacent water drops impacting a liquid film with $v_{drop} = 3.84$ m/s and $h^* = 0.6$. Adapted from Cossali et al. [174].

$$L^* = C\tau^n, \tag{17}$$

as shown in Fig. 22(a) and (b), where the spreading factor L^* is the horizontal spread of the drop normalized by the drop diameter. It should be noted that the exponent in Eq. (17) is $n \approx 0.5$ for $\omega < 0.5$. This power law dependence is similar to that of the crown diameter by Yarin and Weiss [27] as discussed earlier. For spreading on spherical surfaces, Liang et al. [173] defined a spreading factor, A^* , in terms of the spreading area, A_s , normalized by the drop's surface area, A_{drop} ,

$$A^* = \frac{A_s}{A_{drop}}. \tag{18}$$

The experiments by Liang et al. [173] showed that this definition of spreading factor yields a rather linear dependence on non-dimensional time, τ , as shown in Fig. 22(c) and (d), instead of the power law for L^* over cylindrical surfaces.

5.3. Multi-drop impact

Research addressing adjacent-drop impact on a liquid film is an unavoidable step toward understanding the multi-drop interactions prevalent in sprays. Although single-drop research provides a logical foundation for mechanistic understanding of multi-drop impact, the models and correlations developed for single drops cannot be extrapolated to multi-drop impact.

Aside from the secondary droplet formation from single drop impact discussed earlier, secondary drops can result from crown-crown interactions in adjacent drop impacts [17]. Roisman and Tropea [96] examined crown-crown interactions theoretically, using their kinematic discontinuity model discussed earlier. Crown-crown interactions were also observed experimentally for three side-by-side drops by Cossali et al. [174], as shown in Fig. 23. They reported that these interactions accentuate splashing due to more sites being generated for jet formation along the rim of the combined liquid crown. Additionally, splashing was observed to take place below the We threshold for a single drop, and break-up of the liquid sheet generated by the crown-crown interactions yields secondary droplets that are larger than those from a single drop. Barnes et al. [18] named the combined liquid sheet

hump, and investigated its height with respect to the distance between impact centerlines of adjacent drops. They showed that maximum hump height is achieved when this distance is equal to $2d_{drop}$, and that the hump ceases to exist for distances over $3.5d_{drop}$. Their measurements also show that secondary droplets from the hump acquire appreciably lower speeds than those from a single crown.

Xu et al. [90] used 2D simulations to model two drops impacting a thin liquid film, where each drop is represented as a liquid cylinder impacting the film. For successive impact of drops along the same axis, a secondary crown is formed [175], the propagation of which depends on vertical distance between the two drops. For simultaneous impact (*i.e.*, drops impacting the film in unison), a liquid sheet similar to the hump in [18,174] was achieved, the height of which decreases with increasing distance between centerlines of the two drops. Additionally, they computed a large pressure rise in the collision region between the two drops. Similar conclusions were arrived at in the 2D numerical study by Raman et al. [85], who also addressed the effects of film thickness, viscosity ratio, density ratio and velocity for thin moving films.

It is important to point out that simultaneous impact is a 3D problem, which brings into question the validity of findings from 2D simulations. One proof of the limitations of 2D simulations [85,90] is that they predict crown rims extending outwards from the wall with crown angles much smaller than those from experiments. Therefore, future multi-drop impact research must rely on more rigorous 3D simulations that capture the spherical shape of the impacting drops.

Sivakumar and Tropea [17] investigated drop behavior within a spray impacting a liquid film. Their experimental data show a crown proportional to $\tau^{0.2}$, which is considerably different from the $\tau^{0.5}$ dependence obtained by Yarin and Weiss [27] for single drop impact. Sivakumar and Tropea also reported that, even without drop–drop interactions, crown development can be highly asymmetric, which they attributed to spatial variations in film thickness and/or film velocity. For a mono-dispersed spray (*i.e.*, spray with uniformly sized and equal velocity drops) impinging on a film, Ghielmetti et al. [176] correlated the We threshold corresponding to the onset of splashing according to

$$K = WeOh^{-0.4} = 759 + 867h^{*0.15} \quad (19)$$

where $We = 290\text{--}830$, $Oh = 9.9 \times 10^{-3}\text{--}1.2 \times 10^{-2}$ and $h^* = 0.2\text{--}1.2$. The critical We values given by Eq. (19) are lower than those for a single drop, mainly because of multiple drop impact causing increased waviness and shear in the liquid film. These findings prove that multi-drop impact on a film cannot be modeled by superposition of undisturbed single drop impacts.

6. Concluding remarks

This study reviewed published literature addressing the fluid mechanics of a drop impacting a liquid film. Included in the review are depictions of the intermediate stages of evolution of the impact, supported by detailed identification of dominant mechanisms. Key topics discussed are the crown sheet, the ejecta sheet, and splashing for high-velocity impact. Also reviewed are multi-drop impact, and the phenomena of spreading, coalescence and rebound in low-velocity impact. This article also reviewed both the experimental and numerical techniques used by various authors to investigate these mechanisms and phenomena. Key observations from this review can be summarized as follows.

- (1) Recent understanding of drop impact, especially the illusive drop–film neck region, have benefitted greatly from use of advanced experimental methods such as high-

speed imaging and phase-contrast X-ray. Another method that is expected to play a crucial role in future studies is 3D Particle Image Velocimetry (PIV), owing to its ability to provide detailed measurements of liquid flow field. Progress in the understanding of impact behavior is also expected from recent advances in numerical methods. The Coupled Level Set and Volume of Fluid (CLSVOF), Smoothed Particle Hydrodynamics (SPH), and Moving Particle Semi-implicit (MPS) methods are deemed most promising in modeling drop impact, particularly in simulations of the splashing process.

- (2) Aside from impact parameters of the drop and the film, the shape and evolution of the crown are greatly influenced by properties of the surrounding gas and shape and curvature of the solid wall beneath the film. Overall, the kinematic discontinuity theory has been verified both experimentally and numerically as an effective method for describing the formation and evolution of the crown sheet.
- (3) Two primary types of splashing, prompt and delayed, are responsible for formation of secondary droplets. In general, better predictions of splashing thresholds are achieved with relations of the form $K = WeOh^{-0.4}$ than with those based on We alone. The importance of splashing warrants further investigation of the two splashing types, and refinement of splashing thresholds. Overall, experiments involving broad ranges of drop parameters and liquid–gas combinations, aided by new high-speed imaging techniques, are needed to better understand splashing mechanisms and enhance the accuracy of related correlations.
- (4) Several theories have been proposed for dominant mechanisms for the production of secondary droplets by splashing. And despite the popularity of the Rayleigh-Plateau instability and nonlinear amplification as possible mechanisms, there is increasing evidence that splashing is caused by a combination of different instabilities. More careful theoretical, numerical and experimental research is required to identify the true mechanism(s) of splashing for different operating conditions.
- (5) Early moments of the impact are associated with complex interfacial features around the drop–film neck region. Three such features, the ejecta sheet, the adjacent lamella sheet, and the secondary ejecta sheet have been recently captured with aid of X-ray techniques. However, uncertainty remains over such issues as initial formation, speed and emergence time of the ejecta, and the transition from ejecta to random splashing.
- (6) Multi-drop impact has received far less attention than single-drop impact. Much of the multi-drop technical know-how concerns the formation and evolution of a liquid hump from crown–crown interactions of adjacent drops. Overall, multi-drop impact is highly complicated by interaction among drops and increased waviness and shear in the liquid film, and therefore cannot be modeled by superposition of a multitude of single-drop impacts. Multi-drop impact is therefore a topic that warrants significant new experimental and theoretical work.
- (7) Another very important topic that has been widely overlooked in the published literature is heat transfer between a solid wall covered with a liquid film, and an impacting drop or drops. A new field of study is needed that would capitalize upon the present understanding of the fluid mechanics of the impact to determine the heat transfer coefficient associated with sensible heating, interfacial evaporation or interfacial condensation.

Acknowledgements

Support of the National Natural Science Foundation of China (No. 51506023) and China Scholarship Council for this study are gratefully acknowledged.

References

- [1] V. Bergeron, D. Bonn, J.Y. Martin, L. Vovelle, Controlling droplet deposition with polymer additives, *Nature* 405 (6788) (2000) 772–775.
- [2] S.T. Thoroddsen, M.J. Thoraval, K. Takehara, T.G. Etoh, Droplet splashing by a slingshot mechanism, *Phys. Rev. Lett.* 106 (3) (2011) 034501.
- [3] M.R.O. Panão, A.L.N. Moreira, Flow characteristics of spray impingement in PFI injection systems, *Exp. Fluids* 39 (2) (2005) 364–374.
- [4] S. Shen, G. Liang, Y. Guo, R. Liu, X. Mu, Heat transfer performance and bundle-depth effect in horizontal-tube falling film evaporators, *Desalin. Water Treat.* 51 (4–6) (2013) 830–836.
- [5] M. Pasandideh-Fard, S.D. Aziz, S. Chandra, J. Mostaghimi, Cooling effectiveness of a water drop impinging on a hot surface, *Int. J. Heat Fluid Flow* 22 (2) (2001) 201–210.
- [6] D.B. van Dam, C. Le Clerc, Experimental study of the impact of an ink-jet printed droplet on a solid substrate, *Phys. Fluids* 16 (9) (2004) 3403–3414.
- [7] Z. Pan, J.A. Weibel, S.V. Garimella, Influence of surface wettability on transport mechanisms governing water droplet evaporation, *Langmuir* 30 (32) (2014) 9726–9730.
- [8] C. Josserand, S.T. Thoroddsen, Drop impact on solid surface, *Annu. Rev. Fluid Mech.* 48 (2016) 365–391.
- [9] F.H. Harlow, J.P. Shannon, The splash of a liquid drop, *J. Appl. Phys.* 38 (10) (1967) 3855–3866.
- [10] S.L. Manzello, J.C. Yang, An experimental study of a water droplet impinging on a liquid surface, *Exp. Fluids* 32 (5) (2002) 580–589.
- [11] M. Rein, Phenomena of liquid drop impact on solid and liquid surfaces, *Fluid Dyn. Res.* 12 (2) (1993) 61–93.
- [12] J.C. Bird, S.S.H. Tsai, H.A. Stone, Inclined to splash: triggering and inhibiting a splash with tangential velocity, *New J. Phys.* 11 (6) (2009) 063017.
- [13] R. Vander Wal, G. Berger, S. Mozes, The splash/non-splash boundary upon a dry surface and thin fluid film, *Exp. Fluids* 40 (1) (2006) 53–59.
- [14] K. Range, F. Feuillebois, Influence of surface roughness on liquid drop impact, *J. Colloid Interface Sci.* 203 (1) (1998) 16–30.
- [15] Š. Šikalo, E.N. Ganić, Phenomena of droplet–surface interactions, *Exp. Therm. Fluid Sci.* 31 (2) (2006) 97–110.
- [16] Z. Levin, P.V. Hobbs, Splashing of water drops on solid and wetted surfaces: hydrodynamics and charge separation, *Philos. Trans. R. Soc. A Math. Phys. Sci.* 269 (1200) (1971) 555–585.
- [17] D. Sivakumar, C. Tropea, Splashing impact of a spray onto a liquid film, *Phys. Fluids* 14 (12) (2002) L85–L88.
- [18] H.A. Barnes, Y. Hardalupas, A.M.K.P. Taylor, J.H. Wilkins, An investigation of the interaction between two adjacent impinging droplets, in: 15th ILASS-Europe, Toulouse, France, 1999.
- [19] A.L. Yarin, Drop impact dynamics: splashing, spreading, receding, bouncing ..., *Annu. Rev. Fluid Mech.* 38 (1) (2006) 159–192.
- [20] A.L.N. Moreira, A.S. Moita, M.R. Panao, Advances and challenges in explaining fuel spray impingement: how much of single droplet impact research is useful?, *Prog. Energy Combust.* 36 (5) (2010) 554–580.
- [21] A. Prosperetti, H.N. Oguz, The impact of drops on liquid surfaces and the underwater noise of rain, *Annu. Rev. Fluid Mech.* 25 (1) (1993) 577–602.
- [22] C. Tropea, M. Marengo, The impact of drops on walls and films, *Multiphase Sci. Technol.* 11 (1) (1999) 19–36.
- [23] R. Vander Wal, G. Berger, S. Mozes, Droplets splashing upon films of the same fluid of various depths, *Exp. Fluids* 40 (1) (2006) 33–52.
- [24] A.B. Wang, C.C. Chen, Splashing impact of a single drop onto very thin liquid films, *Phys. Fluids* 12 (9) (2000) 2155–2158.
- [25] G.E. Cossali, A. Coghe, M. Marengo, The impact of a single drop on a wetted solid surface, *Exp. Fluids* 22 (6) (1997) 463–472.
- [26] C. Motzkus, F. Gensdarmes, E. Géhin, Parameter study of microdroplet formation by impact of millimetre-size droplets onto a liquid film, *J. Aerosol Sci.* 40 (8) (2009) 680–692.
- [27] A.L. Yarin, D.A. Weiss, Impact of drops on solid surfaces: self-similar capillary waves, and splashing as a new type of kinematic discontinuity, *J. Fluid Mech.* 283 (1995) 141–173.
- [28] C.D. Stow, R.D. Stainer, The physical products of a splashing water drop, *J. Met. Soc. Jpn.* 55 (1977) 518–532.
- [29] C. Mundo, M. Sommerfeld, C. Tropea, Droplet-wall collisions: experimental studies of the deformation and breakup process, *Int. J. Multiphase Flow* 21 (2) (1995) 151–173.
- [30] R. Vander Wal, G. Berger, S. Mozes, The combined influence of a rough surface and thin fluid film upon the splashing threshold and splash dynamics of a droplet impacting onto them, *Exp. Fluids* 40 (1) (2006) 23–32.
- [31] R.D. Deegan, P. Brunet, J. Eggers, Complexities of splashing, *Nonlinearity* 21 (1) (2008) 1–14.
- [32] G. Liang, Y. Guo, S. Shen, Gas properties on crown behavior and drop coalescence, *Numer. Heat Transfer B Fund.* 65 (6) (2014) 537–553.
- [33] A.M. Worthington, A second paper on the forms assumed by drops of liquids falling vertically on a horizontal plate, *Proc. R. Soc. Lond.* 25 (171–178) (1876) 498–503.
- [34] A.M. Worthington, R.S. Cole, Impact with a liquid surface, studied by the aid of instantaneous photography, *Philos. Trans. R. Soc. A* 189 (1897) 137–148.
- [35] A.M. Worthington, R.S. Cole, Impact with a liquid surface studied by the aid of instantaneous photography. Paper II, *Philos. Trans. R. Soc. A* 194 (1900) 175–199.
- [36] H.E. Edgerton, J.R. Killian, *Flash! Seeing the Unseen by Ultra High-speed Photography*, C.T. Branford Co., Boston, 1954.
- [37] S.T. Thoroddsen, T.G. Etoh, K. Takehara, High-speed imaging of drops and bubbles, *Annu. Rev. Fluid Mech.* 40 (2008) 257–285.
- [38] M. Versluis, High-speed imaging in fluids, *Exp. Fluids* 54 (2) (2013) 1–35.
- [39] S. Alghoul, C. Eastwick, D. Hann, Normal droplet impact on horizontal moving films: an investigation of impact behaviour and regimes, *Exp. Fluids* 50 (5) (2011) 1305–1316.
- [40] C.S. Stevens, Scaling of the splash threshold for low-viscosity fluids, *Europhys. Lett.* 106 (2) (2014) 24001.
- [41] E.R. Negeed, M. Albeirutty, Y. Takata, Dynamic behavior of micrometric single water droplets impacting onto heated surfaces with TiO₂ hydrophilic coating, *Int. J. Therm. Sci.* 79 (2014) 1–17.
- [42] E.R. Negeed, S. Hidaka, M. Kohno, Y. Takata, High speed camera investigation of the impingement of single water droplets on oxidized high temperature surfaces, *Int. J. Therm. Sci.* 63 (2013) 1–14.
- [43] B. Peck, L. Sigurdson, The three-dimensional vortex structure of an impacting water drop, *Phys. Fluids* 6 (2) (1994) 564–576.
- [44] H.N. Oguz, A. Prosperetti, Surface-tension effects in the contact of liquid surfaces, *J. Fluid Mech.* 203 (1989) 149–171.
- [45] H.N. Oguz, A. Prosperetti, Bubble entrainment by the impact of drops on liquid surfaces, *J. Fluid Mech.* 219 (1990) 143–179.
- [46] D.A. Weiss, A.L. Yarin, Single drop impact onto liquid films: neck distortion, jetting, tiny bubble entrainment, and crown formation, *J. Fluid Mech.* 385 (1999) 229–254.
- [47] C. Deeney, P. Choi, Novel time and two-dimensional space-resolved X-ray imaging technique, *Rev. Sci. Instrum.* 60 (11) (1989) 3558–3559.
- [48] L.V. Zhang, J. Toole, K. Fezzaa, R.D. Deegan, Evolution of the ejecta sheet from the impact of a drop with a deep pool, *J. Fluid Mech.* 690 (2012) 5–15.
- [49] S.T. Thoroddsen, The ejecta sheet generated by the impact of a drop, *J. Fluid Mech.* 451 (2002) 373–381.
- [50] J.S. Lee, S.J. Park, J.H. Lee, B.M. Weon, K. Fezzaa, J.H. Je, Origin and dynamics of vortex rings in drop splashing, *Nat. Commun.* 6 (2015) 8187.
- [51] J.S. Lee, B.M. Weon, J.H. Je, K. Fezzaa, How does an air film evolve into a bubble during drop impact?, *Phys. Rev. Lett.* 109 (20) (2012) 204501.
- [52] I.V. Roisman, K. Horvat, C. Tropea, Spray impact: rim transverse instability initiating kingering and splash, and description of a secondary spray, *Phys. Fluids* 18 (2006) 102104.
- [53] D. Kalantari, C. Tropea, Phase Doppler measurements of spray impact onto rigid walls, *Exp. Fluids* 43 (2–3) (2007) 285–296.
- [54] G.E. Cossali, M. Marengo, A. Coghe, S. Zhdanov, The role of time in single drop splash on thin film, *Exp. Fluids* 36 (6) (2004) 888–900.
- [55] T. Okawa, T. Shiraiishi, T. Mori, Production of secondary drops during the single water drop impact onto a plane water surface, *Exp. Fluids* 41 (6) (2006) 965–974.
- [56] N. Ninomiya, K. Iwamoto, PIV measurement of a droplet impact on a thin fluid layer, in: The 7th International Symposium on Measurement Techniques for Multiphase Flows, Tianjin, China, 2011, pp. 11–17.
- [57] R. De, A. Karn, J. Noonan, B. Rosiejka, R. Arndt, J. Hong, Characterization of drop impact based on internal flow quantification, in: 68th Annual Meeting of the APS Division of Fluid Dynamics, Boston, Massachusetts, USA, 2015.
- [58] N. Takagaki, S. Komori, Air–water mass transfer mechanism due to the impingement of a single liquid drop on the air–water interface, *Int. J. Multiphase Flow* 60 (2014) 30–39.
- [59] Z. Mohamed-Kassim, E.K. Longmire, Drop coalescence through a liquid/liquid interface, *Phys. Fluids* 16 (7) (2004) 2170–2181.
- [60] B. Richter, K. Dullenkopf, H. Bauer, Investigation of secondary droplet characteristics produced during wall impact, in: Proceedings of the 12th International Symposium Laser Techniques Application Fluid Mechanics, Lisbon, Portugal, 2004.
- [61] B. Richter, K. Dullenkopf, H.-J. Bauer, Investigation of secondary droplet characteristics produced by an isooctane drop chain impact onto a heated piston surface, *Exp. Fluids* 39 (2) (2005) 351–363.
- [62] T. Hori, J. Sakakibara, High-speed scanning stereoscopic PIV for 3D vorticity measurement in liquids, *Meas. Sci. Technol.* 15 (6) (2004) 1067–1078.
- [63] M. Abe, E. Longmire, K. Hishida, M. Maeda, A comparison of 2D and 3D PIV measurements in an oblique jet, *J. Visual.* 3 (2) (2000) 165–173.
- [64] M.P. Arroyo, K. Hinsch, Recent Developments of PIV towards 3D Measurements, Springer, Berlin Heidelberg, 2008, pp. 127–154.
- [65] G. Liang, Y. Guo, S. Shen, Y. Yang, Crown behavior and bubble entrainment during a drop impact on a liquid film, *Theor. Comp. Fluid Dyn.* 28 (2) (2014) 159–170.
- [66] F.H. Harlow, J.E. Welch, Numerical calculation of time-dependent viscous incompressible flow of fluid with free surface, *Phys. Fluids* 8 (1965) 2182–2189.
- [67] C.W. Hirt, B.D. Nichols, Volume of fluid (VOF) method for the dynamics of free boundaries, *J. Comput. Phys.* 39 (1) (1981) 201–225.

- [68] G. Coppola, G. Rocco, L. De Luca, Insights on the impact of a plane drop on a thin liquid film, *Phys. Fluids* 23 (2) (2011) 022105.
- [69] G. Rocco, G. Coppola, L. De Luca, Simulation of drop impact on a thin liquid film by means of the VOF method, *Aerotecnica* 89 (1) (2010) 25–35.
- [70] N. Nikolopoulos, A. Theodorakakos, G. Bergeles, Normal impingement of a droplet onto a wall film: a numerical investigation, *Int. J. Heat Fluid Flow* 26 (1) (2005) 119–132.
- [71] S. Asadi, M. Passandideh-Fard, A computational study of droplet impingement onto a thin liquid film, *Arab. J. Sci. Eng.* 34 (2B) (2009) 505–517.
- [72] M. Rieber, A. Frohn, A numerical study on the mechanism of splashing, *Int. J. Heat Fluid Flow* 20 (5) (1999) 455–461.
- [73] S. Osher, J.A. Sethian, Fronts propagating with curvature-dependent speed: algorithms based on Hamilton–Jacobi formulations, *J. Comput. Phys.* 79 (1) (1988) 12–49.
- [74] S. Lee, N. Hur, S. Kang, A numerical analysis of drop impact on liquid film by using a level set method, *J. Mech. Sci. Technol.* 25 (10) (2011) 2567–2572.
- [75] C. Shao, K. Luo, J. Yang, S. Chen, J. Fan, Accurate level set method for simulations of liquid atomization, *Chin. J. Chem. Eng.* 23 (4) (2015) 597–604.
- [76] M. Sussman, E.G. Puckett, A coupled level set and volume-of-fluid method for computing 3D and axisymmetric incompressible two-phase flows, *J. Comput. Phys.* 162 (2) (2000) 301–337.
- [77] G. Son, Efficient implementation of a coupled level-set and volume-of-fluid method for three-dimensional incompressible two-phase flows, *Numer. Heat Transfer B Fund.* 43 (6) (2003) 549–565.
- [78] B. Ray, G. Biswas, A. Sharma, S.W.J. Welch, CLSVOF method to study consecutive drop impact on liquid pool, *Int. J. Numer. Methods Heat Fluid Flow* 23 (1) (2013) 143–157.
- [79] B. Ray, G. Biswas, A. Sharma, Generation of secondary droplets in coalescence of a drop at a liquid–liquid interface, *J. Fluid Mech.* 655 (2010) 72–104.
- [80] Y. Guo, L. Wei, G. Liang, S. Shen, Simulation of droplet impact on liquid film with CLSVOF, *Int. Commun. Heat Mass Transfer* 53 (2014) 26–33.
- [81] K. Yokoi, A numerical method for free-surface flows and its application to droplet impact on a thin liquid layer, *J. Sci. Comput.* 35 (2) (2008) 372–396.
- [82] D. Zhang, K. Papadikis, S. Gu, Application of a high density ratio lattice-Boltzmann model for the droplet impingement on flat and spherical surfaces, *Int. J. Therm. Sci.* 84 (2014) 75–85.
- [83] S. Shen, F. Bi, Y. Guo, Simulation of droplets impact on curved surfaces with lattice Boltzmann method, *Int. J. Heat Mass Transfer* 55 (23–24) (2012) 6938–6943.
- [84] Z. Shi, Y. Yan, F. Yang, Y. Qian, G. Hu, A lattice Boltzmann method for simulation of a three-dimensional drop impact on a liquid film, *J. Hydrodyn. B* 20 (3) (2008) 267–272.
- [85] K.A. Raman, R.K. Jaiman, T.S. Lee, H.T. Low, On the dynamics of crown structure in simultaneous two droplets impact onto stationary and moving liquid film, *Comput. Fluids* 107 (2015) 285–300.
- [86] S. Mukherjee, J. Abraham, Crown behavior in drop impact on wet walls, *Phys. Fluids* 19 (5) (2007) 052103.
- [87] L.B. Lucy, A numerical approach to the testing of the fission hypothesis, *Astron. J.* 82 (1977) 1013–1024.
- [88] R.A. Gingold, J.J. Monaghan, Smoothed particle hydrodynamics-theory and application to non-spherical stars, *Mon. Not. R. Astron. Soc.* 181 (1977) 375–389.
- [89] S. Koshizuka, H. Tamako, Y.A. Oka, A particle method for incompressible viscous flow with fluid fragmentation, *J. Comput. Fluid Dyn.* 4 (1995) 29–46.
- [90] X. Xu, J. Ouyang, T. Jiang, Q. Li, Numerical analysis of the impact of two droplets with a liquid film using an incompressible SPH method, *J. Eng. Math.* 85 (1) (2014) 35–53.
- [91] H. Xie, S. Koshizuka, Y. Oka, Modelling of a single drop impact onto liquid film using particle method, *Int. J. Numer. Methods Fluids* 45 (9) (2004) 1009–1023.
- [92] N. Nikolopoulos, A. Theodorakakos, G. Bergeles, Three-dimensional numerical investigation of a droplet impinging normally onto a wall film, *J. Comput. Phys.* 225 (1) (2007) 322–341.
- [93] R. Rioboo, C. Bauthier, J. Conti, M. Voué, J. De Coninck, Experimental investigation of splash and crown formation during single drop impact on wetted surfaces, *Exp. Fluids* 35 (6) (2003) 648–652.
- [94] G. Liang, Y. Guo, S. Shen, Analysis of liquid sheet and jet flow mechanism after droplet impinging onto liquid film, *Acta Phys. Sin.* 62 (2) (2013) 024705.
- [95] M.F. Trujillo, C.F. Lee, Modeling crown formation due to the splashing of a droplet, *Phys. Fluids* 13 (9) (2001) 2503–2516.
- [96] I.V. Roisman, C. Tropea, Impact of a drop onto a wetted wall: description of crown formation and propagation, *J. Fluid Mech.* 472 (2002) 373–397.
- [97] H. Shetabivash, F. Ommi, G. Heidarinejad, Numerical analysis of droplet impact onto liquid film, *Phys. Fluids* 26 (1) (2014) 012102.
- [98] J. Guo, X. Wang, Simulation of the two phase flow of droplet impingement on liquid film by the lattice Boltzmann method, *J. Hydrodyn. B* 24 (2) (2012) 292–297.
- [99] G. Liang, Y. Guo, Y. Yang, S. Guo, S. Shen, Special phenomena from a single liquid drop impact on wetted cylindrical surfaces, *Exp. Therm. Fluid Sci.* 51 (2013) 18–27.
- [100] G. Liang, Y. Guo, Y. Yang, S. Shen, Liquid sheet behaviors during a drop impact on wetted cylindrical surfaces, *Int. Commun. Heat Mass Transfer* 54 (2014) 67–74.
- [101] X. Gao, R. Li, Impact of a single drop on a flowing liquid film, *Phys. Rev. E* 92 (5) (2015) 053005.
- [102] A. Coghe, G. Brunello, G.E. Cossali, M. Marengo, Single drop splash on thin film: measurements of crown characteristics, in: 15th ILASS-Europe, Toulouse, France, 1999.
- [103] M.R. Davidson, Spreading of an inviscid drop impacting on a liquid film, *Chem. Eng. Sci.* 57 (17) (2002) 3639–3647.
- [104] C. Josserand, S. Zaleski, Droplet splashing on a thin liquid film, *Phys. Fluids* 15 (6) (2003) 1650–1657.
- [105] G. Agbaglah, R.D. Deegan, Growth and instability of the liquid rim in the crown splash regime, *J. Fluid Mech.* 752 (2014) 485–496.
- [106] H. Fujimoto, T. Ogino, H. Takuda, N. Hatta, Collision of a droplet with a hemispherical static droplet on a solid, *Int. J. Multiphase Flow* 27 (7) (2001) 1227–1245.
- [107] W.C. Macklin, G.J. Metaxas, Splashing of drops on liquid layers, *J. Appl. Phys.* 47 (9) (1976) 3963–3970.
- [108] A.I. Fedorchenko, A.B. Wang, On some common features of drop impact on liquid surfaces, *Phys. Fluids* 16 (5) (2004) 1349–1365.
- [109] J. Guo, S. Dai, Q. Dai, Experimental research on the droplet impacting on the liquid film, *Acta Phys. Sin.* 59 (4) (2010) 2601–2609.
- [110] K.L. Pan, K.R. Cheng, P.C. Chou, C.H. Wang, Collision dynamics of high-speed droplets upon layers of variable thickness, *Exp. Fluids* 45 (3) (2008) 435–446.
- [111] E. Berberović, N.P. van Hinsberg, S. Jakirlić, I.V. Roisman, C. Tropea, Drop impact onto a liquid layer of finite thickness: dynamics of the cavity evolution, *Phys. Rev. E* 79 (3) (2009) 036306.
- [112] I.V. Roisman, N.P. van Hinsberg, C. Tropea, Propagation of a kinematic instability in a liquid layer: capillary and gravity effects, *Phys. Rev. E* 77 (4) (2008) 046305.
- [113] N.P. van Hinsberg, M. Budakli, S. Göhler, E. Berberović, I.V. Roisman, T. Gambaryan-Roisman, C. Tropea, P. Stephan, Dynamics of the cavity and the surface film for impingements of single drops on liquid films of various thicknesses, *J. Colloid Interface Sci.* 350 (1) (2010) 336–343.
- [114] N.L. Hillen, J.M. Kuhlman, M. Dinc, D.D. Gray, Drop impingement on wet and dry surfaces, in: 42nd AIAA Fluid Dynamics Conference and Exhibit, New Orleans, USA, 2012.
- [115] J.M. Kuhlman, N.L. Hillen, M. Dinc, D.D. Gray, Liquid volume measurements in the cavity formed by single droplet impacts into a thin, static liquid film, *Exp. Therm. Fluid Sci.* 54 (2014) 179–188.
- [116] C. Motzkus, F. Gensdarmes, E. Géhin, Study of the coalescence/splash threshold of droplet impact on liquid films and its relevance in assessing airborne particle release, *J. Colloid Interface Sci.* 362 (2) (2011) 540–552.
- [117] G. Liang, Y. Guo, Y. Yang, N. Zhen, S. Shen, Spreading and splashing during single drop impact on an inclined wetted surface, *Acta Mech.* 224 (12) (2013) 2993–3004.
- [118] C. Motzkus, E. Géhin, F. Gensdarmes, Study of airborne particles produced by normal impact of millimetric droplets onto a liquid film, *Exp. Fluids* 45 (5) (2008) 797–812.
- [119] L.V. Zhang, J. Toole, K. Fezzaa, R.D. Deegan, Splashing from drop impact into a deep pool: multiplicity of jets and the failure of conventional scaling, *J. Fluid Mech.* 703 (2012) 402–413.
- [120] L. Xu, W. Zhang, S.R. Nagel, Drop splashing on a dry smooth surface, *Phys. Rev. Lett.* 94 (18) (2005) 184505.
- [121] L. Xu, L. Barcos, S.R. Nagel, Splashing of liquids: interplay of surface roughness with surrounding gas, *Phys. Rev. E* 76 (6) (2007) 066311.
- [122] M.M. Driscoll, S.R. Nagel, Ultrafast interference imaging of air in splashing dynamics, *Phys. Rev. Lett.* 107 (15) (2011) 154502.
- [123] T. Okawa, T. Shiraishi, T. Mori, Effect of impingement angle on the outcome of single water drop impact onto a plane water surface, *Exp. Fluids* 44 (2) (2008) 331–339.
- [124] Š. Šikalo, C. Tropea, E.N. Ganić, Impact of droplets onto inclined surfaces, *J. Colloid Interface Sci.* 286 (2) (2005) 661–669.
- [125] K.L. Pan, C.Y. Hung, Droplet impact upon a wet surface with varied fluid and surface properties, *J. Colloid Interface Sci.* 352 (1) (2010) 186–193.
- [126] L. Ma, M. Liu, J. Chang, T. Su, H. Liu, Numerical simulation of droplet impact onto liquid films with smoothed particle hydrodynamics, *Acta Phys. Sin.* 61 (24) (2012) 244701.
- [127] M. Marengo, C. Tropea, Aufprall von Tropfen auf flüssigkeitsfilme, *Tr* 194/10, 1999, 1, 2.
- [128] Q. Huang, H. Zhang, A study of different fluid droplets impacting on a liquid film, *Petrol. Sci.* 5 (1) (2008) 62–66.
- [129] P. Walzel, Zerteilgrenze beim Tropfenprall, *Chem. Ing. Tech.* 52 (1980) 338–339.
- [130] M.M. Driscoll, C.S. Stevens, S.R. Nagel, Thin film formation during splashing of viscous liquids, *Phys. Rev. E* 82 (3) (2010) 036302.
- [131] P. Tsai, R. Van Der Veen, M. Van Dde Raa, D. Lohse, How micropatterns and air pressure affect splashing on surfaces, *Langmuir* 26 (20) (2010) 16090–16095.
- [132] A. Latka, A. Strandburg-Peshkin, M.M. Driscoll, C.S. Stevens, S.R. Nagel, Creation of prompt and thin-sheet splashing by varying surface roughness or increasing air pressure, *Phys. Rev. Lett.* 109 (5) (2012) 054501.
- [133] H. Vu, D. Banks, G. Aguilar, Examining viscosity and surface wettability on lamella lift dynamics and droplet splashing, *Atomization Spray* 21 (4) (2011) 303–315.
- [134] L.V. Zhang, P. Brunet, J. Eggers, R.D. Deegan, Wavelength selection in the crown splash, *Phys. Fluids* 22 (12) (2010) 122105.
- [135] O.G. Engel, Initial pressure, initial flow velocity, and the time dependence of crater depth in fluid impacts, *J. Appl. Phys.* 38 (10) (1967) 3935–3940.
- [136] P.H. Gregory, E.J. Guthrie, M.E. Bunce, Experiments on splash dispersal of fungus spores, *J. Gen. Microbiol.* 20 (2) (1959) 328–354.

- [137] P.V. Hobbs, T. Osheroff, Splashing of drops on shallow liquids, *Science* 158 (3805) (1967) 1184–1186.
- [138] R.F. Allen, The mechanics of splashing, *J. Colloid Interface Sci.* 124 (1) (1988) 309–316.
- [139] L. Rayleigh, On the capillary phenomena of jets, *Proc. R. Soc. Lond.* 29 (196–199) (1879) 71–97.
- [140] J.M. Fullana, S. Zaleski, Stability of a growing end rim in a liquid sheet of uniform thickness, *Phys. Fluids* 11 (1999) 952–954.
- [141] N. Bremond, E. Villermaux, Atomization by jet impact, *J. Fluid Mech.* 549 (2006) 273–306.
- [142] G. Lagubeau, M.A. Fontelos, C. Josserand, A. Maurel, V. Pagneux, P. Petitjeans, Flower patterns in drop impact on thin liquid films, *Phys. Rev. Lett.* 105 (18) (2010) 184503.
- [143] R.D. Deegan, P. Brunet, J. Eggers, Rayleigh-Plateau Instability Causes the Crown Splash, 2008, pp. 1–4. arXiv: 0806.3050v2.
- [144] G. Taylor, The dynamics of thin sheets of fluid. III. Disintegration of fluid sheets, *Proc. R. Soc. A Math. Phys.* 253 (1959) 313–321.
- [145] A.L. Yarin, *Free Liquid Jets and Films: Hydrodynamics and Rheology*, Longman Publishing Group, New York, 1993, p. 446.
- [146] I.V. Roisman, T. Gambaryan-Roisman, O. Kyriopoulos, P. Stephan, C. Tropea, Breakup and atomization of a stretching crown, *Phys. Rev. E* 76 (2) (2007) 026302.
- [147] I.V. Roisman, On the instability of a free viscous rim, *J. Fluid Mech.* 661 (2010) 206–228.
- [148] D. Gueyffier, S. Zaleski, Finger formation during droplet impact on a liquid film, *C.R. Acad. Bulg. Sci.* 326 (12) (1998) 839–844.
- [149] R. Krechetnikov, G.M. Homsy, Crown-forming instability phenomena in the drop splash problem, *J. Colloid Interface Sci.* 331 (2) (2009) 555–559.
- [150] M. Brouillette, The Richtmyer–Meshkov instability, *Annu. Rev. Fluid Mech.* 34 (1) (2002) 445–468.
- [151] G. Agbaglah, C. Josserand, S. Zaleski, Longitudinal instability of a liquid rim, *Phys. Fluids* 25 (2) (2013) 022103.
- [152] R. Krechetnikov, Stability of liquid sheet edges, *Phys. Fluids* 22 (9) (2010) 092101.
- [153] S.T. Thoroddsen, T.G. Etoh, K. Takehara, Crown breakup by Marangoni instability, *J. Fluid Mech.* 557 (2006) 63–72.
- [154] S.D. Howison, J.R. Ockendon, J.M. Oliver, R. Purvis, F.T. Smith, Droplet impact on a thin fluid layer, *J. Fluid Mech.* 542 (2005) 1–23.
- [155] M.J. Thoraval, K. Takehara, T.G. Etoh, S.T. Thoroddsen, Drop impact entrapment of bubble rings, *J. Fluid Mech.* 724 (2013) 234–258.
- [156] A.A. Castrejón-Pita, J.R. Castrejón-Pita, I.M. Hutchings, Experimental observation of von Karman vortices during drop impact, *Phys. Rev. E* 86 (4) (2012) 045301.
- [157] M.J. Thoraval, K. Takehara, T.G. Etoh, S. Popinet, P. Ray, C. Josserand, S. Zaleski, S.T. Thoroddsen, Von Kármán vortex street within an impacting drop, *Phys. Rev. Lett.* 108 (26) (2012) 264506.
- [158] S.T. Thoroddsen, The making of a splash, *J. Fluid Mech.* 690 (2012) 1–4.
- [159] S. Chandra, C.T. Avedisian, On the collision of a droplet with a solid surface, *Proc. R. Soc. A Math. Phys.* 432 (1884) (1991) 13–41.
- [160] W.M. Healy, J.G. Hartley, S.I. Abdel-Khalik, On the validity of the adiabatic spreading assumption in droplet impact cooling, *Int. J. Heat Mass Transfer* 44 (20) (2001) 3869–3881.
- [161] S. Herbert, S. Fischer, T. Gambaryan-Roisman, P. Stephan, Local heat transfer and phase change phenomena during single drop impingement on a hot surface, *Int. J. Heat Mass Transfer* 61 (2013) 605–614.
- [162] Z. Zhao, D. Poulikakos, J. Fukai, Heat transfer and fluid dynamics during the collision of a liquid droplet on a substrate. I. Modeling, *Int. J. Heat Mass Transfer* 39 (13) (1996) 2771–2789.
- [163] G. Strotos, M. Gavaises, A. Theodorakakos, G. Bergeles, Numerical investigation of the cooling effectiveness of a droplet impinging on a heated surface, *Int. J. Heat Mass Transfer* 51 (19–20) (2008) 4728–4742.
- [164] M. Rein, The transitional regime between coalescing and splashing drops, *J. Fluid Mech.* 306 (1996) 145–165.
- [165] H. Aryafar, H. Kavehpour, Drop coalescence through planar surfaces, *Phys. Fluids* 18 (7) (2006) 072105.
- [166] F. Blanchette, T.P. Bigioni, Dynamics of drop coalescence at fluid interfaces, *J. Fluid Mech.* 620 (2009) 333–352.
- [167] X. Chen, S. Mandre, J.J. Feng, Partial coalescence between a drop and a liquid–liquid interface, *Phys. Fluids* 18 (5) (2006) 051705.
- [168] A. Karl, A. Frohn, Experimental investigation of interaction processes between droplets and hot walls, *Phys. Fluids* 12 (4) (2000) 785–796.
- [169] D. Chowdhury, S.P. Sarkar, D. Kalita, T.K. Sarma, A. Paul, A. Chattopadhyay, Spreading and recoil of a surfactant-containing water drop on glass-supported alcohol films, *Langmuir* 20 (4) (2004) 1251–1257.
- [170] G. Liang, S. Shen, Y. Guo, J. Chen, H. Yu, Y. Li, Special phenomena of droplet impact on an inclined wetted surface with experimental observation, *Acta Phys. Sin.* 62 (8) (2013) 084707.
- [171] G. Liang, Y. Yang, Y. Guo, N. Zhen, S. Shen, Rebound and spreading during a drop impact on wetted cylinders, *Exp. Therm. Fluid Sci.* 52 (2014) 97–103.
- [172] G. Liang, Y. Guo, S. Shen, Observation and analysis of drop impact on wetted spherical surfaces with low velocity, *Acta Phys. Sin.* 62 (18) (2013) 184703.
- [173] G. Liang, Y. Guo, X. Mu, S. Shen, Experimental investigation of a drop impacting on wetted spheres, *Exp. Therm. Fluid Sci.* 55 (2014) 150–157.
- [174] G.E. Cossali, M. Marengo, M. Santini, Impact of single and multiple drop array on a liquid film, in: *Proceeding of the 19th ILASS-Europe*, Nottingham, UK, 2004.
- [175] T. Zhang, J. Muthusamy, J.L. Alvarado, A. Kanjirakat, R. Sadr, Numerical and experimental investigations of crown propagation dynamics induced by droplet train impingement, *Int. J. Heat Fluid Flow* 57 (2016) 24–33.
- [176] C. Ghielmetti, M. Marengo, T. Steigleder, C. Tropea, Droplet impingement on a solid surface covered by a liquid film, in: *13th Annual Conference on Liquid Atomisation and Spray Systems, ILASS-Europe*, Florence, Italy, 1997, pp. 465–472.